Fuel 364 (2024) 131078

Contents lists available at ScienceDirect

Fuel

journal homepage: www.elsevier.com/locate/fuel

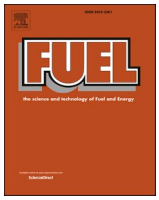

Full Length Article

Laminar burning Velocities, Markstein numbers and cellular instability of spherically propagation Ethane/Hydrogen/Air premixed flames at elevated pressures

Jinzhou Li, Yu Xie, Mohamed Elsayed Morsy, Junfeng Yang *

School of Mechanical Engineering, University of Leeds, Leeds LS2 9JT, United Kingdom

ARTICLE INFO

Keywords:
Laminar premixed flame
Laminar burning velocities
Ethane-Hydrogen blends
Cellular instabilities
Markstein length

ABSTRACT

Laminar flame characteristics of ethane/hydrogen/air (with X_{H_2} = 25 %, 50 %, 75 % and 100 % by volume) within an equivalence ratio from 0.7 to 1.3 were determined in a spherical constant volume combustion vessel at elevated pressure up to 0.5 MPa, temperature up to 360 K. Key combustion characteristics such laminar burning velocity, Markstein length/number, flame thickness, effective Lewis number, thermal expansion coefficient and critical conditions at the onset of cellular instability including critical radius and Peclet number, were either measured or calculated. These measurements were compared with the available literature data and with the predictions from chemical kinetics mechanisms, showing perfect fitting with the literature data, although the kinetics were overpredicted at a temperature of 360 K. The dependence of the ethane/hydrogen/air laminar burning velocities on temperature, pressure, and hydrogen ratio was analyzed using a datum empirical expression and blending law, yielding excellent agreement. A general correlation, based on the Peclet number against the Markstein number, has been proposed for various mixtures and conditions, aimed at defining the stable and unstable regimes of flame propagation. This correlation exhibits an R^2 value of 0.82, signifying a strong predictive capacity. The findings highlight that, compared with methane, ethane plays a promising role in enhancing the resistance of hydrogen mixtures to cellular flame instability, thereby fostering more stable flame propagation.

1. Introduction

In the UK, over 70 % of primary energy is derived from the combustion of primary liquid and gaseous fuels, primarily natural gas, which comprises mostly of methane and varying amounts of higher alkanes such as ethane and propane [1]. As of 2022, natural gas combustion accounted for more than 40 % of the country's electricity generation. Ethane, being the second most abundant component in natural gas after methane, varies in composition from 0.5 % to 13.3 % by volume and plays a crucial role in petrochemical production, particularly as a feedstock for ethylene production, and is also used in power generation [2]. Notably, there has been a significant global increase in ethane storage, attributed to its enhanced usage and production. For instance, ethane production in the U.S. surged by 250 %, increasing from 3×10^8 barrels into 7.5×10^8 barrels between 2010 and 2022 [3]. The mounting concerns regarding finite oil reserves and atmospheric pollution have catalyzed a rising interest in the utilization of ethane mixtures in combustion engines and power generation systems. Compared to methane, ethane exhibits faster burning velocities and more stable flames, resulting in higher thermal efficiencies when utilized in engines [4–6].

The laminar burning velocities (LBV) of pure ethane-air mixture have been extensively studied. Lowry et al. [7] measured the laminar burning velocity of pure ethane, methane and ethane/methane mixtures over a wide range of equivalence ratio from 0.7 to 1.3 in a constant-volume optical cylindrical vessel with initial pressure of 0.1, 0.5 and 1 MPa. It was shown that compared with methane/air, ethane/air mixtures have higher laminar burning velocity. For example, under 300 K, 0.1 MPa condition stochiometric ethane/air have LBV of 0.39 m/s higher than the stochiometric methane/air with 0.33 m/s. Mitu et al. [8] measured the normal burning velocity and propagation speed of ethane/air via cubic law of pressure rise to study the effects of temperature dependence. Nilsson et al. [9] implemented the heat flux method to study the effects of hydrogen addition on the laminar burning velocities of methane/ethane/propane hydrocarbon blends and presented that the

* Corresponding author.
E-mail address: J.Yang@leeds.ac.uk (J. Yang).

https://doi.org/10.1016/j.fuel.2024.131078
Received 17 November 2023; Received in revised form 21 January 2024; Accepted 24 January 2024

Nomenclature

A	Laminar flame surface area (m^2)
k	Thermal conductivity (W/(m·K))
L_b	Markstein length on the burned side of the flame (mm)
Ma_b	Markstein number on the burned side
Ma_{sr}	Markstein number associated to aerodynamic strain
Pe_{cl}	Critical Peclet number
P_0	Datum atmospheric pressure (0.1 MPa)
Pr	Prandtl number
r_{cl}	Critical flame radius (mm)
r_u	Cold flame radius (mm)
R_{sch}	Front radius obtained by Schlieren ciné-photography (mm)
S_n	Stretched flame speed (m/s)
S_s	Flame speed at zero stretch rate (m/s)
T_0	Datum atmospheric temperature (300 K)
u_l	Unstretched laminar burning velocity (m/s)
$u_{l,0}$	Datum unstretched laminar burning velocity at T_0 and P_0
V_{H_2}	Hydrogen volume fraction
$V_{C_2H_6}$	Ethane volume fraction
X_{H_2}	Volumetric percentage of Hydrogen
Ze	Zel'dovich number

Greek symbols

α	Flame stretch rate (1/s)
α_T	Temperature coefficients for u_l
β_P	Pressure coefficients for u_l
δ_l	Laminar flame thickness (mm) ν/u_l
ν	Unburnt gas kinematic viscosity (m^2/s)
ρ_u	Unburnt gas density (kg/m^3)
ρ_b	Burnt gas density (kg/m^3)
ϕ	Equivalence ratio

addition of hydrogen can enhance the laminar burning velocity. Most recently, Goswami et al. [10] conducted the experimental and modelling method to measure the laminar burning velocity of ethane/air and propane/air at elevated pressure up to 0.4 MPa with a wild range of equivalence ratio from 0.8 to 1.3. The study of Ravi et al. [11] also measured the laminar burning velocity of pure ethane and analyzed the enhancement LBV of ethane and ethylene addition on the methane. Methane blends with ethylene yielded higher flame speeds when compared to those containing ethane. Zuo et al. [12] reported the effects of initial pressure on the self-acceleration characteristics of laminar C1-C3 alkane/air premixed mixtures using spherically expanding flames and the results show that the both acceleration exponent and fractal dimension of C1-C3 alkane increased with the increasing pressure. Similarly, Zuo et al. [13] studied the cellular instabilities of laminar premixed C1-C3 alkane/air mixture under a wide range of initial pressure (0.25–1.5 MPa) in a constant volume combustion vessel and the results showed that the increasing of initial pressure will enhance the hydrodynamic instability of these three alkane-air mixtures.

Compared with hydrocarbons, hydrogen stands out as a key player due to its zero carbon emissions, demonstrating unique laminar flame characteristics. These include high reactivity, rapid laminar burning velocities, and flame instabilities, even occurring at low pressures and relatively small flame radii [14]. It is known that the instability of hydrogen flame increases with increasing initial, pressure and decreasing Markstein number, flame thickness and non-monotonically varies with increasing equivalence ratio [14–17]. The appropriate addition of hydrogen into hydrocarbons can facilitate ignition, enhance combustion intensity, and optimize combustion systems such as gas turbines and engines, resulting in reduced pollutant emissions and improved performance and operational ranges [18–20]. However, adding to much hydrogen addition into hydrocarbon may prone to unwanted pre-ignition, knock and high level of NO_x emission in engines [21]. Therefore, a thorough understanding of the combustion characteristics associated with hydrogen addition to hydrocarbons is essential.

Numerous studies have been conducted to investigate the impact of hydrogen addition on various hydrocarbon flames in terms of LBV, Markstein length and flame cellular instability. Law and Kown [22] focused on the effects of methane, ethylene, and propane additions to hydrogen flames, discovering that the addition of C1-C3 hydrocarbons could reduce both the laminar burning velocity and flame temperature, contributing to a more stable flame. Building on this, Law et al. [23] carried out a more nuanced study, specifically exploring the impact of propane addition on hydrogen/air flames. Their findings suggested that propane addition inhibits the development of flame instabilities. Marwaan et al. [24] investigated the effects of hydrogen addition on the laminar burning velocities, Markstein number on methane with pressure up to 10 bar in combustion vessel and the laminar burning velocities increase with initial temperature and hydrogen additions. Similarly, Mohamed and Yang [16], focusing on cellular instabilities of methane/hydrogen/air flame, observed that augmenting initial pressure and hydrogen fractions led to earlier onset of wrinkling in the flame fronts, highlighting a trend toward increased flame instability. Li et al. [25] extended research on ammonia/hydrogen/air mixtures laminar flame properties using the spherical flame propagation method in a constant volume chamber, finding that hydrogen addition elevates LBVs and enhances global flame instability due to thermal and chemical kinetic impacts.

However, the effects of hydrogen additions on the ethane laminar premixed flame remain unclear, requiring a comprehensive understanding of the effects of hydrogen additions, equivalence ratio, temperature, and pressure on the LBV, Markstein length/number, and cellular flame instability of ethane/hydrogen/air flames. Here, the Markstein length describes the effect of the stretch rate on the burning velocity. A large value of Markstein length is indicative of a strong effect of stretch rate on the burning velocity, conversely for the small Markstein length [26]. Where the Markstein number, Ma_b, is the dimensionless parameter which is ratio of Markstein length, L_b, divided by the flame thickness, δ_l. Although various correlations have been proposed to define stable and unstable flames, such as those involving hydrogen [14], methane [27], methane/hydrogen/air [16,24], and propane/hydrogen/air [23], combining these data with current measurements of ethane/hydrogen/air mixtures would be valuable. It allows for the proposal of a general dimensionless correlation, facilitating the classification of stable and unstable flame regimes across diverse fuel compositions. Different chemical mechanisms related to the laminar burning velocity of small hydrocarbon methane and ethane have been developed in several research groups, e.g. Aramco Mech 1.3 [28], GRI 3.0 mechanism [29], San Diego mechanism [30], and the USC Mech Version II [31]. In general, the prediction of these chemical mechanisms was consistent only within a certain range of initial conditions and fuels. Therefore, measurements of the laminar burning velocity of ethane/hydrogen/air flames can serve as a database for further improvement of these mechanisms and as input for numerical simulations.

Thus, to fill the knowledge gaps and owing such considerations, the objectives of present study are: (i) providing the measured combustion characteristics data including LBVs, burned gas Markstein length and number and instability parameters critical radius and Peclet number for ethane/hydrogen/air over a wide equivalence ratio from 0.7 to 1.3, initial pressure from 0.1 MPa to 0.5 MPa, initial temperature from 300 K to 360 K and hydrogen addition with 25 %, 50 % and 75 % by volume. (ii) The experimental results of laminar burning velocity are used in this study to compare with the results from chemical kinetics mechanism

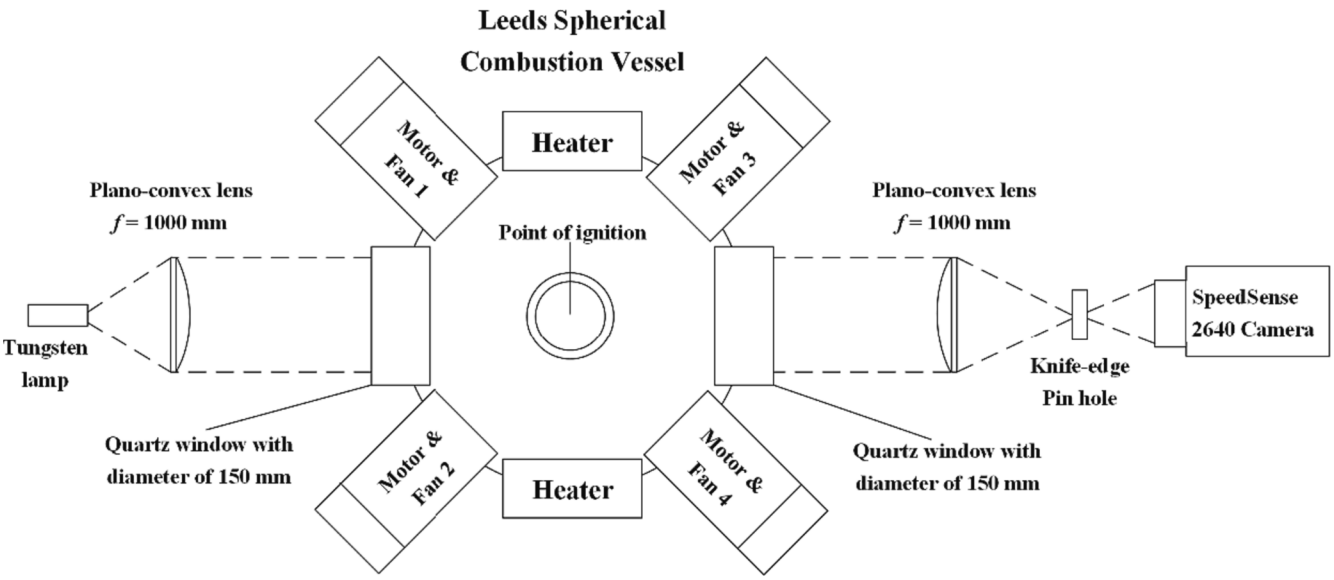

Fig. 1. Schematic of the Leeds Spherical combustion vessel and Schlieren ciné set-up.

Table 1
Laminar propagation flame experimental conditions for ethane/hydrogen/air mixtures.

Mix Type (X_{H_2})	Equivalence ratio	Temperature (K)	Pressure (MPa)
0 %	0.7, 0.8, 0.9, 1.0, 1.1, 1.2, 1.3	300, 360	0.1 and 0.5
25 %		300	0.1
50 %		300, 360	0.1 and 0.5
75 %		300	0.1
100 %		300	0.1

(iii) The correlations describing the effects of initial temperature, pressure and hydrogen additions on the laminar burning velocity of ethane/hydrogen/air is developed in this study. (iv) A general correlation defines the stable regime for the propagation of hydrogen/air, methane/hydrogen/air and ethane/hydrogen/air flame based on the dependences of Pe_{cl} and Ma_b is reported in this study.

2. Methodology

A spherical stainless-steel fan-stirred constant-volume combustion vessel with 380-mm-diameter, Leeds MK-II [24,25,29], has been used for the laminar flame characteristics measurement in this study (see Fig. 1). The Leeds MK-II vessel has two pairs of orthogonal windows with 150 mm diameter. Two 2 kW internal coiled electric heaters which mounted inside wall of the vessel were equipped to heat the vessel and mixtures to 360 K and the initial temperature was measured by a sheathed Type K thermocouple made from a 25 μ Chromel-Alumel wire. A static pressure transducer (Druck PDCR 911) which mounted flush to the inner wall of the vessel connecting with an LCD display was used to measure the absolute pressure in the vessel during the mixture preparation. The combustion vessel was equipped with four identical, eight-bladed fans which arranged in a tetrahedron formation. Four fans driven by four 8 kW electric motors with independent and accurate speed control, which were used to achieve the homogenously fuel/air mixtures before the ignition.

The pressure during combustion was measured by a dynamic Kistler pressure transducer (Kistler 701A) which mounted flush to the inner wall of the vessel and the pressure signal was amplified and recorded by a Kistler 5007 change amplifier, at a sampling rate of 50 kHz. A centrally positioned spark plug was mounted though the vessel wall with minimum ignition energies of about 0.5 mJ, which supplied from a 12 V transistorized automotive ignition coil system. This spark plug was used to ignite all mixtures in this study. The combustible ethane/hydrogen (X_{H_2} = 0 %, 25 %, 50 %, 75 % and 100 % hydrogen by volume) mixtures were prepared quantitively in the combustion vessel with concentrations based on the partial pressure method. The purities of ethane and hydrogen were 99.9 % and 99.95 % respectively. The experimental conditions and mixtures are shown in Table. 1 below.

The volumetric percentage of hydrogen X_{H_2} based on the volume of ethane/hydrogen/air mixtures was calculated as: $X_{H_2} = V_{H_2}/(V_{H_2} + V_{C_2H_6})$, where V_{H_2} and $V_{C_2H_6}$ are the hydrogen and ethane volume fractions in the fuel blends, respectively. The total equivalence ratio ϕ is calculated as:

$$\phi = \frac{F/A}{(F/A)_{st}} \tag{1}$$

where (F/A) is the total fuel to air ratio and $(F/A)_{st}$ is the stochiometric value of fuel to air ratio. The chemical combustion formular for stoichiometric ethane/hydrogen/air mixtures can be expressed as:

$$(1 - X_{H_2})C_2H_6 + X_{H_2}H_2 + (\frac{3.5}{\phi}(1 - X_{H_2}) + \frac{X_{H_2}}{2\phi})(O_2 + 3.76N_2) \tag{2}$$

The flame propagation images were recorded by Schlieren ciné photography to obtain the flame radius, flame speeds, stretch rates, Markstein length, number and Peclet number. The Schlieren ciné apparatus utilized a 150-watt adjustable tungsten lamp (MI-150 Dolan-Jenner), functioning as a near-point light source expanded onto an f-1000 mm plano-convex lens. This setup collimated a 150 mm beam, allowing it to pass through the vessel and its contents, directed to another f-1000 mm plano-convex lens. Consequently, this lens focused the beam onto a knife-edge pinhole with a 0.5 mm diameter, projecting directly onto a high-speed digital camera (SpeedSense 2640, DANTEC DYNAMICS Co., Ltd, UK). The camera operated at speeds of 10,000 frames/s, offering a resolution of 512x512 pixels and 0.265 mm/pixel.

Schlieren images were processed by using a MATLAB code [32] which employed in previous studies [14,16,24,33]. This code detects flame edges to distinguish the burned and unburned regions. In the processed images, the unburnt gas regions are subtracted, leaving with black, while the regions with burnt gases processed as white. The flame area is subsequently calculated by counting the number of pixels in the white region, allowing for the determination of an equivalent flame radius, r_{sch}. For each experimental condition, three experiments were

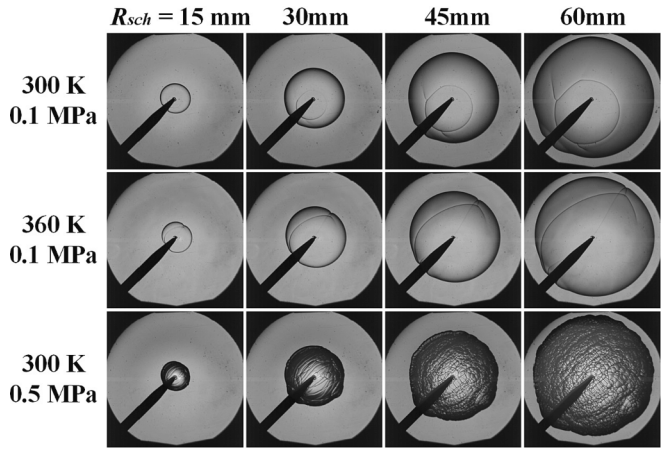

Fig. 2. Schlieren images showing the effects of initial temperature and pressure on the developments of laminar ethane/air flames with $\phi = 1.1$.

performed to ensure repeatability. Average values from sets of three experiments were used, to increase the certainty of our measurements. The standard deviation error bar was defined to be the square root of the variance (a sum of squared deviation divided by the number of data points, 3, for each test condition). The error bars were plotted around the mean values in all experimental results.

The flame speed is defined as the measured flame radius against time by:

$$S_n = \frac{dr_u}{dt} \tag{3}$$

where r_u is the cold flame radius and defined as the 5 K above the temperature of reactants [27]. The computational study of spherical flame propagation [34] reported that cold flame radius is related to the Schlieren observed flame radius r_{sch} and is expressed as:

$$r_u = r_{sch} + 1.95\delta_l\left(\frac{\rho_u}{\rho_b}\right)^{0.5} \tag{4}$$

where ρ_u is the unburned density of mixture, ρ_b is the burned density of mixtures and their value are derived from the GasEq code [35]. δ_l is the laminar flame thickness given as $\delta_l = \frac{\nu}{u_l Pr}$, ν is the kinematic viscosity, P_r is the Prandtl number $P_r = \frac{\nu}{\alpha}$ where here α is the thermal diffusivity. The kinematic viscosity and thermal diffusivity of ethane-air and ethane-hydrogen-air mixtures were all derived from GasEq code. For the spherical flame measurements, the total stretch rate acting on the flame with surface area, A, is defined as:

$$\alpha = \frac{1}{A}\frac{dA}{dt} = \frac{2}{r_u}\frac{dr_u}{dt} = \frac{2}{r_u}S_n \tag{5}$$

The burned gas Markstein length, L_b, is adpoted here to quantify the linear regression between flame speed and total stretch rate [26]:

$$S_s - S_n = L_b\alpha \tag{6}$$

where S_s is the unstretched flame speed which is the extrapolated flame speed at zero stretch rate and it derived from the stable flame with linear relationship between S_n and α by using Eq. (6). The laminar burning velocity is derived from unstretched flame speed and for constant pressure flame propagation it defined as:

$$u_l = S_s\frac{\rho_b}{\rho_u} \tag{7}$$

The nonlinear extrapolation method which emphasizes the nonlinear variation of S_n to α, as proposed by Kelley and Law [36], was also implemented in this study. This method was used to derive S_s and to make comparisons with linear extrapolation. The expression for this nonlinear extrapolation is as follows:

$$\left(\frac{S_n}{S_s}\right)^2 ln\left(\frac{S_n}{S_s}\right)^2 = -2\frac{L_b\alpha}{S_S} \tag{8}$$

However, the occurrence of hydrodynamics (Darrieus-Landau) and thermo-diffusive instability cause the cellular structure on the flame surface and accelerate the burning velocity [33,37]. The Peclect number, Pe_{cl}, is applied here as the critical dimensionless group to quantify the onset of cellular instability and it expressed as:

$$Pe_{cl} = \frac{r_{cl}}{\delta_l} \tag{9}$$

where, r_{cl}, is the critical flame radius at which the sudden emergence of cell structure over the flame surface. All these parameters were measured in the present study. The hydrodynamic flame instability arises from density discontinuities when the flame interacts with hydrodynamic disturbances. The hydrodynamics instability is governed by two parameters thermal expansion coefficient, σ, across the flame front and laminar flame thickness, δ_l, where the $\sigma = \frac{\rho_u}{\rho_b}$ is the ratio of burned to unburned gas density. The hydrodynamic instability increases with a larger thermal expansion ratio and a thinner flame thickness. Based on the study by Kwon et al. [38], it has been found that the stretching effect of the flame front can inhibit the cellular development of flames with positive curvature. A thinner flame results in a diminished effect of curvature stretching, enhancing the hydrodynamics instability. Additionally, in wrinkled flames, laminar flame thickness plays a crucial role in controlling the intensity gradient of the baroclinic torque, which is generated by the density and pressure gradients across the flame surface. A reduction in flame thickness leads to an increase in the density gradient, subsequently amplifying the hydrodynamic instability due to the heightened intensity of the baroclinic torque. The influence of thermal-diffusive instability on a flames surface is quantified using the Lewis number,*Le*. The Lewis number is defined as follows:

$$Le = \frac{D_T}{D_M} = \frac{\lambda}{\rho_u c_p D_M} \tag{10}$$

where, λ is the thermal conductivity, c_p is the specific heat at constant pressure, D_M is the mass diffusive coefficient of unburned mixture. A Lewis number of one ($Le = 1$) implies that there is no influence of thermal-diffusive instability on the overall flame instability. However, a Lewis number less than one ($Le < 1$) indicates that the flame is becoming unstable due to the effects of thermal-diffusive instability, and vice versa. Following the [39–41], for the ethane/hydrogen/air mixtures, the effective Lewis number is calculated using the volume-weighted method,

$$Le_{eff} = X_{H_2}Le_{H_2} + X_{C_2H_6}Le_{C_2H_6} \tag{11}$$

where, Le_{H_2} and $Le_{C_2H_6}$ are the Lewis number of hydrogen and ethane, respectively. In this study, the numerical modeling of laminar burning velocities in an ethane/hydrogen/air flame environment is conducted using CHEMKIN-PRO software [42]. A one-dimensional, freely propagating laminar flame model is employed, leveraging two common detailed chemical kinetics mechanisms: Aramco Mech 1.3 [28] and USC Mech II [31]. These mechanisms are employed to conduct a comparative analysis against the current measurements of laminar burning velocities of ethane/hydrogen/air flames.

3. Results and discussion

3.1. Effect of stretch rate on the flame speed

The effect of both temperature and pressure on the propagation of ethane/air flames with $\phi = 1.1$ is illustrated in Fig. 2. At 0.1 MPa, the

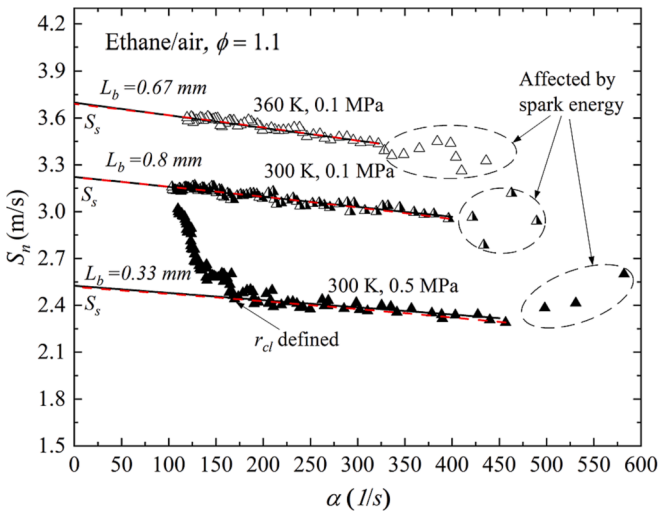

Fig. 3. Variations of measured flame speeds, S_n, with stretch rate,α, for the conditions of Fig. 2. (solid black line representing the linear extrapolation, red dashed line representing the nonlinear extrapolation). (For interpretation of the references to colour in this figure legend, the reader is referred to the web version of this article.)

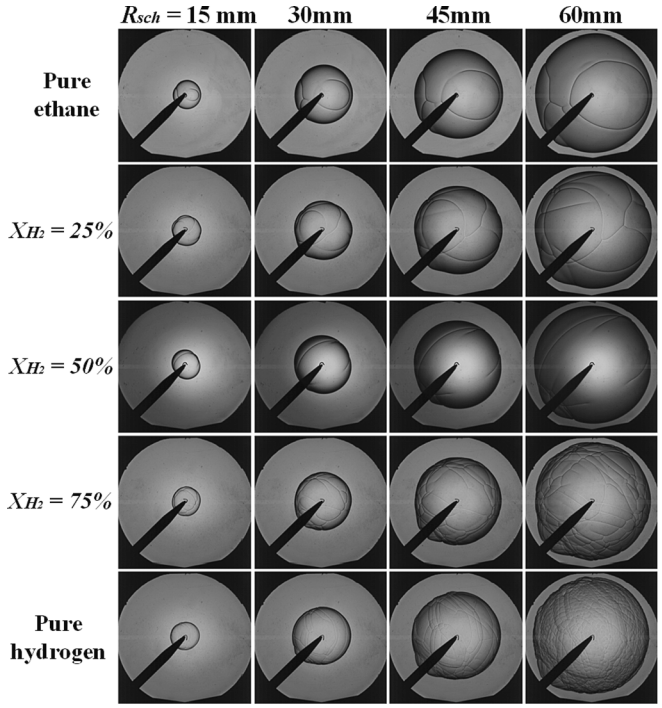

Fig. 4. Schlieren images showing the effects of hydrogen additions on the developments of stochiometric laminar ethane/hydrogen/air flame at 300 K and 0.1 MPa.

smooth spherical flame was observed with no cracking and cellular structure on flame surface even the radius reaching 60 mm. While, at 0.5 MPa and 300 K, the cracks is first observed at 15 mm, as the flame expanding the cellular structure occurred at 45 mm.

Compared with temperature, clearly the pressure dominates the flame cellular instability of ethane/air mixtures, this tendency consistent with others hydrocarbons for example, methane/air [27], ethanol/air [43], and even with the hydrogen/air flame [14]. Law et al. [23] explained that cellular instability is enhanced with increasing initial pressure. The rise in initial pressure decreases the flame thickness,

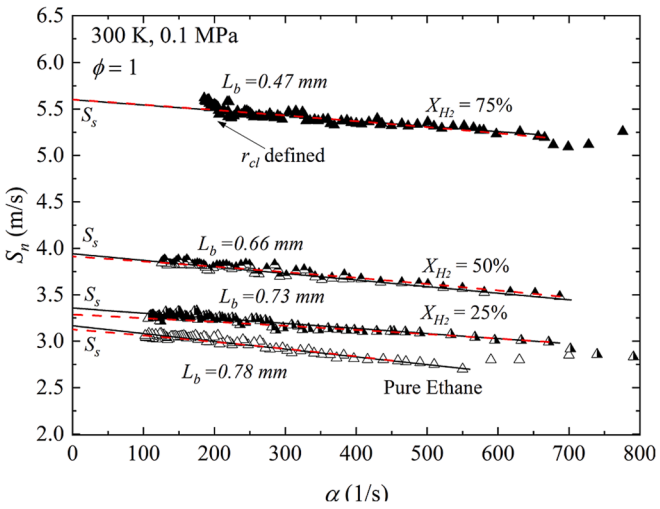

Fig. 5. Variations of measured flame speeds, S_n, with stretch rate,α, for the conditions of Fig. 4. (solid black line representing the linear extrapolation, red dashed line representing the nonlinear extrapolation). (For interpretation of the references to colour in this figure legend, the reader is referred to the web version of this article.)

which in turn, enhances the effects of hydrodynamic instability.

To better understand the effect of stretch rate on flame speed and instability, the variations of flame speed against the stretch rate for different initial pressures and temperatures were presented in Fig. 3. To select a valid range of flame radius for extrapolating the upstretched laminar flame speed, S_S, the influences of ignition energy, vessel wall effects, and cellular instability have to be considered. For cases without cellular instability, the flame radius was set within the range of 10 mm < r_{sch} < 55 mm. The choice of a flame radius larger than 10 mm in our study is corroborated by the findings of Bradley et al. [26,44], which indicate that while the flame speed is initially influenced by ignition energy, it attains independence from these effects once the flame radius exceeds 6 mm. Additionally, the upper limit of 55 mm for the flame radius was chosen in accordance with the 380 mm diameter of our combustion vessel. This decision aligns with the findings of Burke et al. [45], who suggest that wall effects can be largely disregarded when the flame radius is less than 0.3 times the radius of the vessel wall. At a pressure of 5 MPa, and in the presence of large radii and small stretch, the flames reach the limit of stable propagation. Beyond this point, the flames become unstable and cellular due to the effects of flame hydrodynamic instability, leading to an increase in surface area and consequent acceleration of the flames. As show in Fig. 3, the critical radius r_{cl} marks the onset of cellular instability for the condition 0.5 MPa, 300 K. In scenarios exhibiting cellular instability, the flame radius range was selected to be within 10 mm < r_{sch} < r_{cl}.

The stable regime for the determination of Markstein lengths, L_b lies between these points. Both linear (Eq.6) and nonlinear (Eq.8) extrapolations were implemented to drive the unstretched flame speeds. The comparison of both methods was shown in Figs. 3 and 5 with various mixtures and conditions as the black solid line representing the linear extrapolation, the red dashed line representing the nonlinear extrapolation. The comparison indicates that both methods yield nearly identical unstretched flame speeds with negligible differences in the current measurements. Therefore, the linear method presents simplicity and convenient of use, in this study the classic linear extrapolation method was adopted to determine the unstretched LBV. The unstretched flame speeds, S_s, have been derived by linear extrapolation at zero stretch rate and the gradient of solid line represents the -L_b. As illustrated in Fig. 3, there is a noticeable relationship between the initial conditions and the S_s. An increase in the initial temperature is observed to enhance S_s, while a rise in initial pressure appears to suppress the S_s. This suppression is

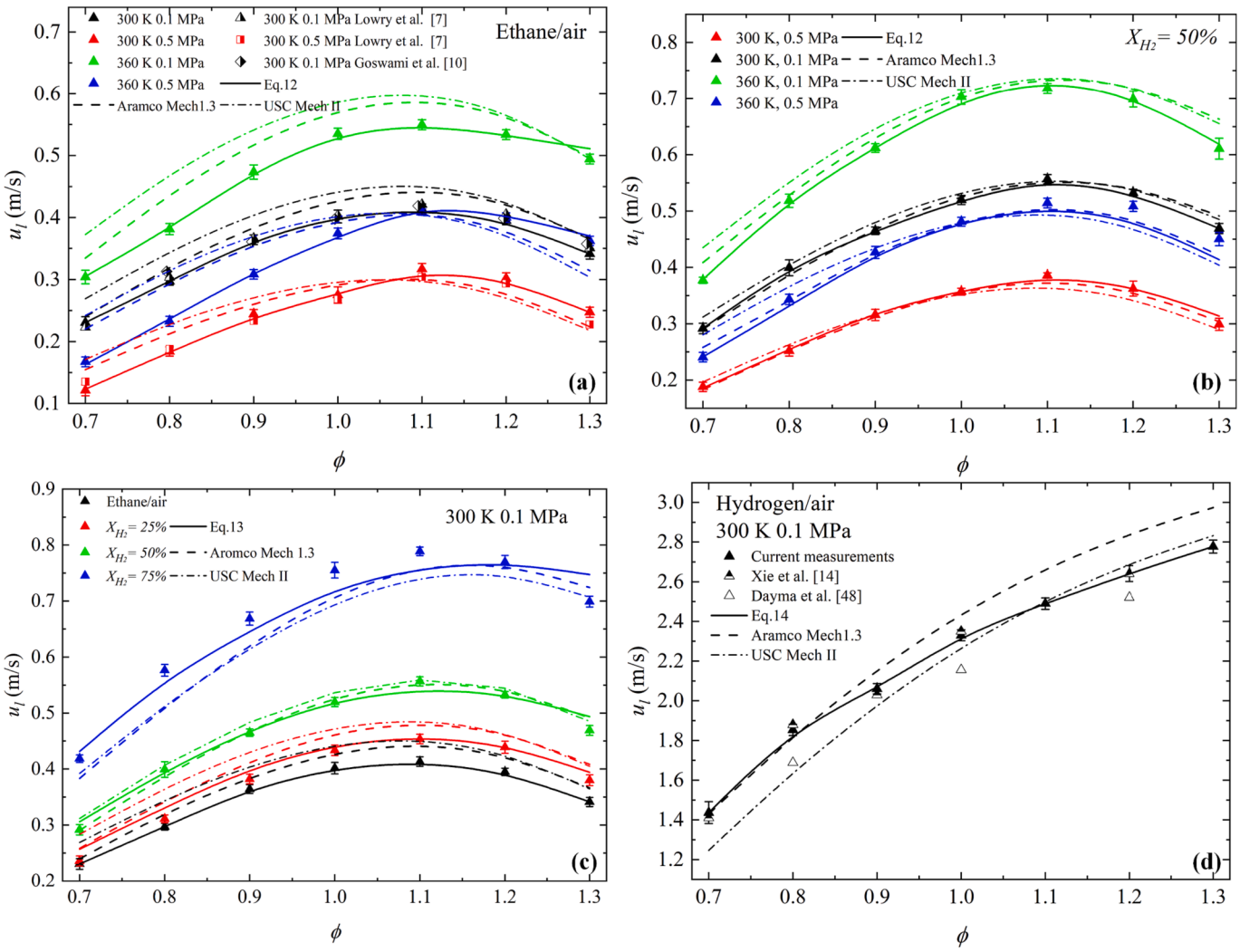

Fig. 6. Laminar burning velocity of ethane/hydrogen/air at conditions in Table.1. (The solid lines, dashed lines, dashed dot lines represent the u_l from Eq. (12) and Eq.13, Aramco Mech 1.3 [28] and USC Mech II [31]).

attributed to reduction of flame thickness due to the rising pressure conditions.

The effects of hydrogen additions (X_{H_2} = 0 %, 25 %, 50 %, 75 % and 100 %) on the flame propagation of ethane/hydrogen/air mixtures with ϕ = 1.0, 0.1 MPa and 300 K as shown in Fig. 4. The smooth spherical flame was observed with no cracking and cellular even the radius reaching 60 mm for mixtures with $X_{H_2} \leq 50$ %. As X_{H_2} = 75 %, the large crack is first observed at 30 mm, and no cellular structure until the flame reaching 60 mm. While, the pure hydrogen flame shows the strongest instability, the large crack starts at 30 mm radius and cellular structure occurs at 60 mm radius with small cells on the flame surface.

Fig. 5 shows the effects of hydrogen additions on the flame speed against with stretch rate. The unstretched flame speed is increasing with the hydrogen addition, while Markstein lengths, L_b, decreases with the increasing hydrogen additions.

3.2. Unstretched laminar burning velocity

The unstretched laminar burning velocities of ethane/hydrogen/air mixtures at conditions in Table.1 are presented in Fig. 6. In the case of a pure ethane/air mixture, as illustrated in subplot (a), the peak laminar burning velocity is observed at a temperature of 360 K and a pressure of 0.1 MPa with an equivalence ratio of 1.1. Under these conditions, the laminar burning velocity reaches a maximum value of 0.55 m/s. The increases of initial temperature leading to the increase of laminar burning velocity while the pressure shows the opposite effect. The measured laminar burning velocities of ethane/air mixtures by Lowry et al. [7] and Goswami et al. [10] are plotted along with the present work and showing a very good agreement with current measurements for the full range of equivalence ratio. The predicted laminar burning velocities, as determined using the Aramco Mech 1.3 and USC Mech II mechanisms, are distinctly represented in Fig. 6 with dashed and dashed-dot lines, respectively. Overall, the predictions made by both the Aramco Mech 1.3 and USC Mech II mechanisms align satisfactorily with the current measurements at 300 K. However, there is an overprediction observed at 360 K across a full range of equivalence ratios at 0.5 MPa, and when $\phi \leq 0.9$ at 0.1 MPa. This discrepancy could be attributed to the limited validation of the Aramco Mech 1.3 mechanism [28], which has been corroborated only using data from Lowry [7] concerning pressure-dependent burning velocity at 300 K, 0.1 and 0.5 MPa. Similarly, the USC Mech II has been validated solely with the laminar burning velocities of ethane/air from references [46,47] at 300 K and 0.1 MPa. To achieve accurate predictions regarding the laminar flame propagation of ethane/air mixtures, it is recommended that both mechanisms be further refined and validated against the high temperature experimental data. Moreover, the solid line in Fig. 6 (a) and (b) represents the laminar burning velocity from the correlation (Eq.12) which consider the effects of pressure and temperature and compared

Table 2
The value of $u_{l,0}$, α_T and β_P for pure ethane/air mixtures with ϕ from 0.7 to 1.3.

ϕ	$u_{l,0}$	α_T	β_P
0.7	0.231	1.53	−0.39
0.8	0.297	1.38	−0.30
0.9	0.364	1.44	−0.26
1	0.402	1.57	−0.23
1.1	0.413	1.57	−0.17
1.2	0.395	1.64	−0.17
1.3	0.341	2	−0.2

Table 3
The value of $u_{l,0}$, α_T and β_P for ethane/hydrogen/air ($X_{H2} = 50$ %) mixtures with ϕ from 0.7 to 1.3.

ϕ	$u_{l,0}$	α_T	β_P
0.7	0.292	1.43	−0.28
0.8	0.399	1.44	−0.28
0.9	0.465	1.52	−0.23
1	0.52	1.62	−0.23
1.1	0.557	1.52	−0.23
1.2	0.533	1.53	−0.23
1.3	0.469	1.52	−0.25

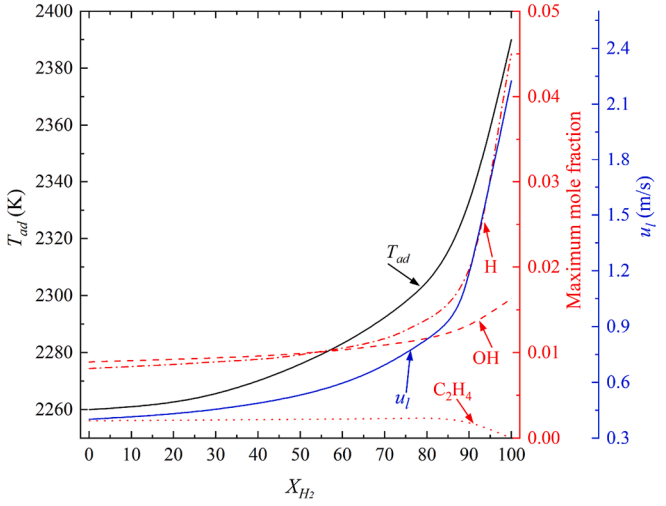

Fig. 7. The modelling adiabatic flame temperature and maximum mole fraction of H, OH, C_2H_4 radicals as a function of hydrogen ratio at 300 K, 0.1 MPa and $\phi = 1$.

with the kinetics this correlation can perfectly fit with the measured data.

The laminar burning velocities of ethane/hydrogen/air flames ($X_{H_2} = 50$ %) at initial temperatures of 300 and 360 K, and pressures of 0.1 and 0.5 MPa, are depicted in Fig. 6 (b). Given the absence of reported experimental data for ethane/hydrogen/air in existing literature, the currently measured data have been compared with predictions made by both mechanisms. It is observed that the laminar burning velocities predicted by both mechanisms align well with the measured data, showing a good level of agreement. The effects of hydrogen additions ($X_{H_2} = 25$ %, 50 % and 75 % by volume) on the laminar burning velocity of ethane at 300 K, 0.1 MPa are presented in Fig. 6 (c). The laminar burning velocity increases with increasing hydrogen ratio for all equivalence ratio. For all hydrogen additions, the maximum laminar burning velocity appears at $\phi = 1.1$. It is apparent the modelling results from both mechanisms overpredict at $X_{H_2} = 25$ %, underpredict at $X_{H_2} = 75$ % and good fitting at$X_{H_2} = 50$ %. This is may be because the ethane kinetics become predominant at low hydrogen addition ($X_{H2} \leq 25$ %). This error caused the noticeable discrepancy between modelling and measurement. Thus, the blending law, based on the mass fraction from Eq. (13) and presented as a solid line, is proposed, showing good fitting with the measured data. The laminar burning velocity of pure hydrogen/air was measured and shown in Fig. 6 (d). The data measured in the present study are represented by solid triangle symbols and compared with data from Xie et al. [14] and Dayma et al. [48]. The current measurements align perfectly with Xie et al. [14], but are approximately 10 % higher than the measurements from Dayma et al. [48]. Additionally, the predicted results from both mechanisms show satisfactory agreement with the measured.

3.3. Correlation of laminar burning velocity

The comparative study reveals that both the Aramco MECH 1.3 and USC Mech II mechanisms are only validated under certain conditions, showing limited performance in predicting the laminar burning velocity of ethane/hydrogen/air mixtures at 360 K. Thus, empirical correlations of laminar burning velocity considering the effects of temperature and pressure becomes a matter of urgency. Metghalchi and Keck [49] proposed a laminar burning velocity correlation which consider the effects of temperature and pressure on laminar burning velocity under datum conditions shown in Eq. (12), and this correlation is used to show the effects of temperature and pressure on laminar burning velocity of methane/air [27] and *i*-octane/*n*-heptane/air mixtures [34].

$$u_l = u_{l,0}\frac{T_u^{\alpha_T}}{T_0}\frac{P_u^{\beta_P}}{P_0} \tag{12}$$

where, $u_{l,0}$ presents the laminar burning velocity at a datum temperature $T_0 = 300$ K and $P_0 = 0.1$ MPa in the current measurements. The constants α_T and β_P act as the temperature and pressure exponents, respectively, with a positive value indicating an increasing effect on the laminar burning velocity and vice versa. These constants, dependent on the equivalence ratio, represent the influence of temperature and pressure on the laminar burning velocity of the ethane/air mixture, as delineated in Table 2.

The correlation for the ethane/hydrogen/air ($X_{H_2} = 50$ %) mixtures is also purposed in this study. The values of $u_{l,0}$, α_T and β_P for this mixture are shown in Table. 3 below. The solid lines in Fig. 6 (a) and (b) represent the laminar burning velocity from this correlation and it is shown that the value from correlation is good fitting with the measured laminar burning velocity.

For the effect of hydrogen addition on the laminar burning velocity of ethane, the blending law based on the mass fraction of mixture reported in [50] is used in this study and expressed as:

$$u_l = x_i u_{li} + x_j u_{lj} \tag{13}$$

where x_i is the mass fraction of the i-th ingredient mixture within the overall mass and u_{li} is the laminar burning velocity of i-th ingredient mixture. The same definitions apply to the j-th ingredient. For the ethane/hydrogen/air mixture, in terms of volume fraction, Eq. (13) can be reformulated as:

$$u_l = \frac{2X_{H_2}}{2X_{H_2} + 30(1 - X_{H_2})}u_{lH_2} + \frac{30(1 - X_{H_2})}{2X_{H_2} + 30(1 - X_{H_2})}u_{lC_2H_6} \tag{14}$$

where u_{lH_2} and $u_{lC_2H_6}$ are the laminar burning velocity of hydrogen and ethane respectively. The solid line in Fig. 6 (c) and (d) displays the values of the laminar burning velocity derived from the blending law, demonstrating a good fit with the measured data.

3.4. Thermal and chemical kinetics effects

The addition of hydrogen to ethane/air mixtures results in an increase in the laminar burning velocity. This is attributed to the positive influence of hydrogen addition on the overall thermal and chemical

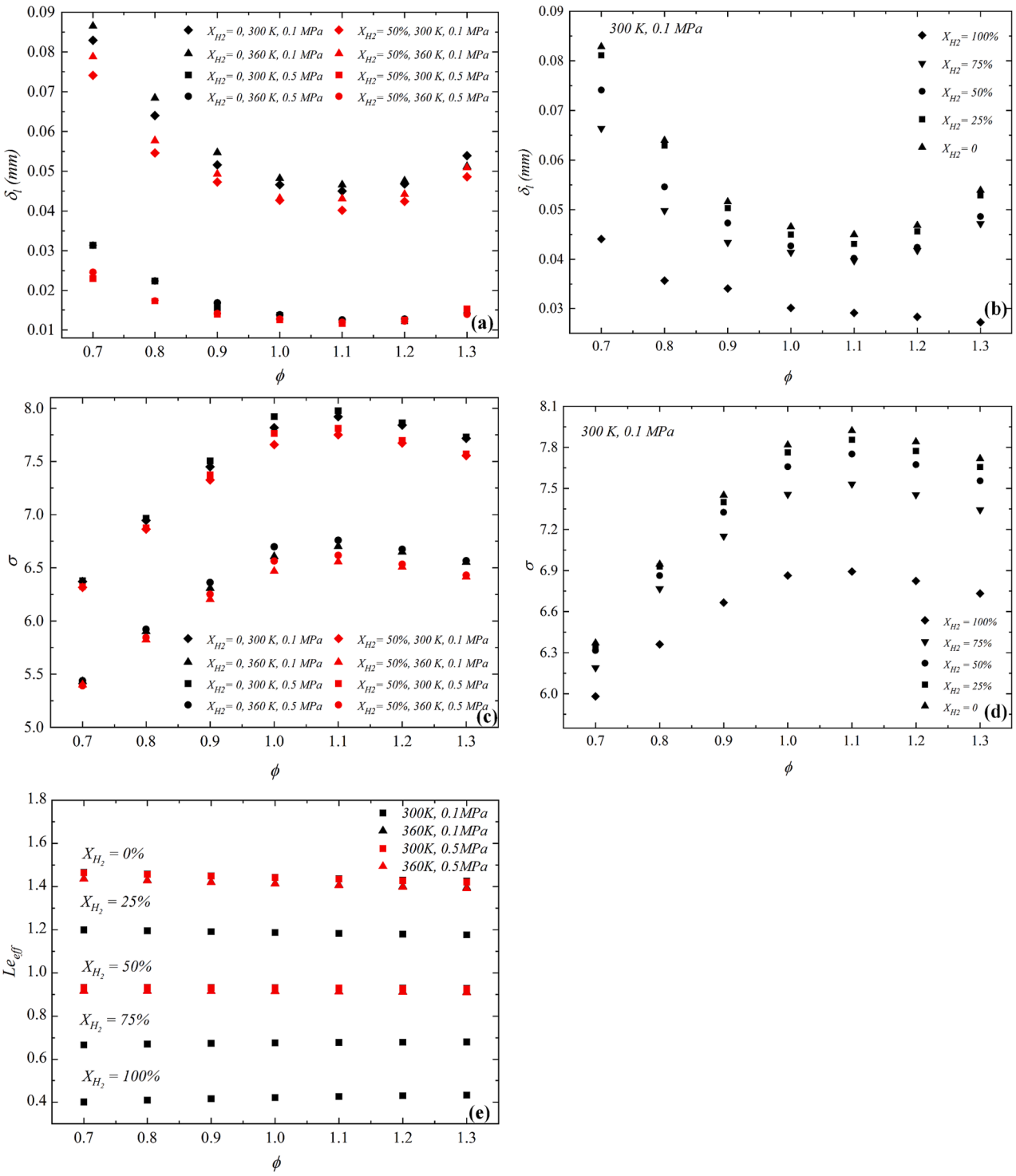

Fig. 8. The variation of the flame thickness, δ_l, thermal expansion coefficient, σ, and the effective Lewis number, Le_{eff} of ethane/hydrogen/air mixture at 300 K and 360 K under pressures of 0.1 and 0.5 MPa, as functions of the equivalence ratio.

kinetics effects [51]. Here, the thermal effects are represented by the adiabatic flame temperature T_{ad} and key radicals can be used to characterized the chemical kinetics effect [51]. Radicals such as H and OH are predominant in promoting the laminar burning velocity, while the C_2H_4 radical signifies the decomposition of ethane. Consequently, T_{ad}, u_l and maximum mole fraction of H, OH, C_2H_4 radicals are illustrated against X_{H_2} at 300 K, 0.1 MPa and $\phi = 1$ in Fig. 7. This aims to demonstrate the impact of hydrogen addition on both thermal and chemical kinetics effects. Where the T_{ad} and maximum mole fractions of radicals are calculated using a one-dimensional, freely propagating laminar flame model from the CHEMKIN-PRO software [42], in conjunction with Aramco Mech 1.3 [28]. Meanwhile, the u_l values are form the current measurements.

Overall, the T_{ad}, u_l and maximum mole fraction of H, OH radicals show an increasing trend with the X_{H_2}, while the C_2H_4 radicals display the opposite trend. The T_{ad} increases with X_{H_2}, ranging from 2260 K for ethane/air to 2390 K for hydrogen/air. This indicates an enhancement of thermal effects with the increase in X_{H_2}, accompanied by a rise in u_l.

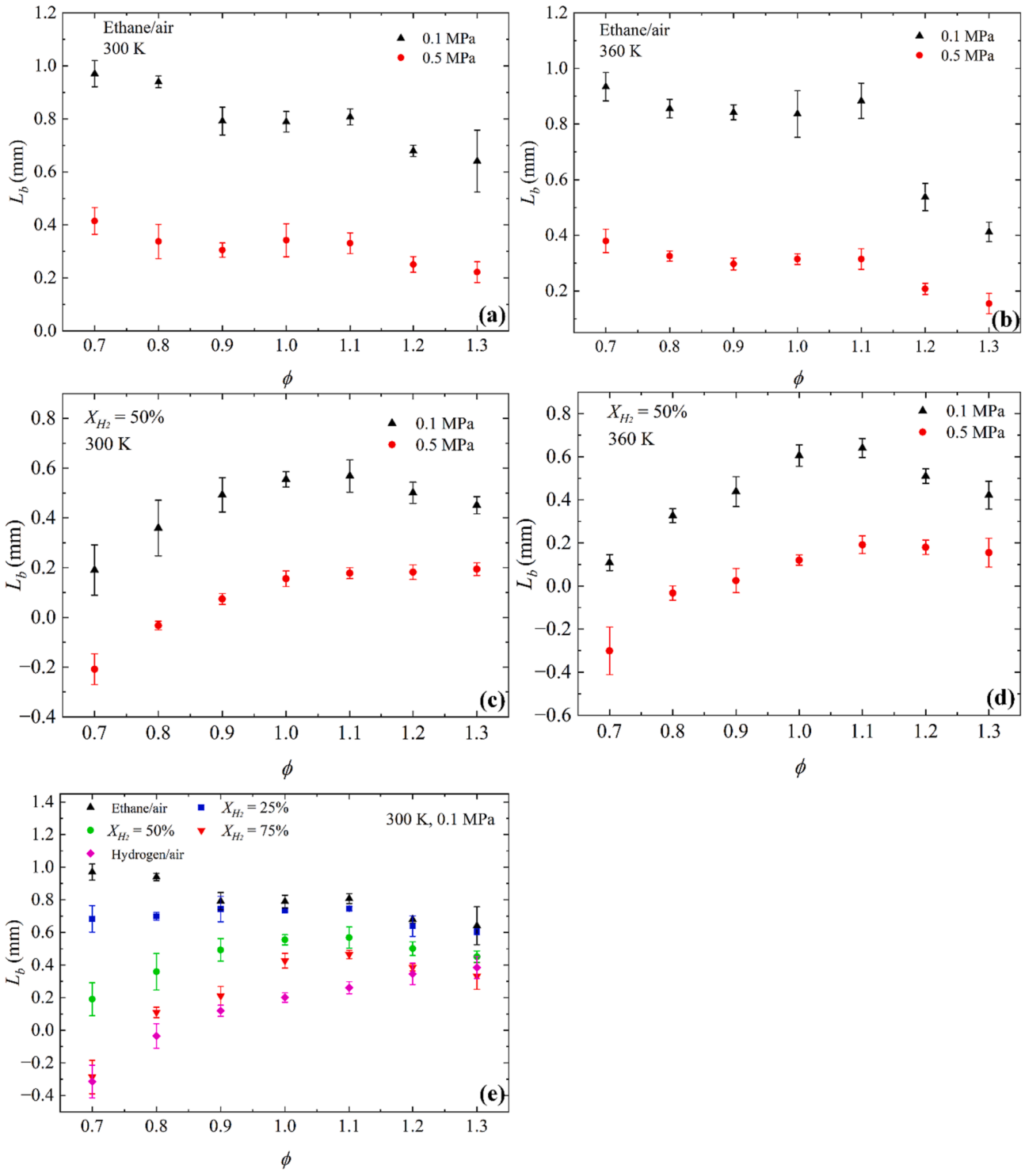

Fig. 9. The variations of measured burned gas Markstein length, L_b, of ethane/hydrogen/air mixtures with equivalence ratio, ϕ, at temperature of 300, 360 K, and pressure of 0.1, 0.5 MPa.

The maximum mole fractions of H and OH radicals also escalate swiftly with X_{H_2}, with the H radicals, in particular, showing exponential growth when$X_{H_2} > 90$ %. This signifies an amplification of the chemical kinetics effects with X_{H_2}. Conversely, the maximum mole fractions of C_2H_4 radicals moderately increase with X_{H_2} up to 50 %, then decline due to the reduced ethane content in the fuel. Hence, an increase in X_{H_2} amplifies both thermal and chemical effects, resulting in an elevated laminar burning velocity of ethane/hydrogen/air mixtures.

3.5. Flame thickness, thermal expansion coefficient and effective Lewis number

In previous discussion, the flame thickness, δ_l, thermal expansion coefficient, σ, dominate the hydrodynamic instability and the effective Lewis number, Le_{eff} were identified as dominant factors influencing thermal-diffusive instability. These parameters, in the context of ethane/hydrogen/air, are illustrated in Fig. 8. Referring to Fig. 8 (a) and (b) concerning flame thickness, it is observed that the flame thickness

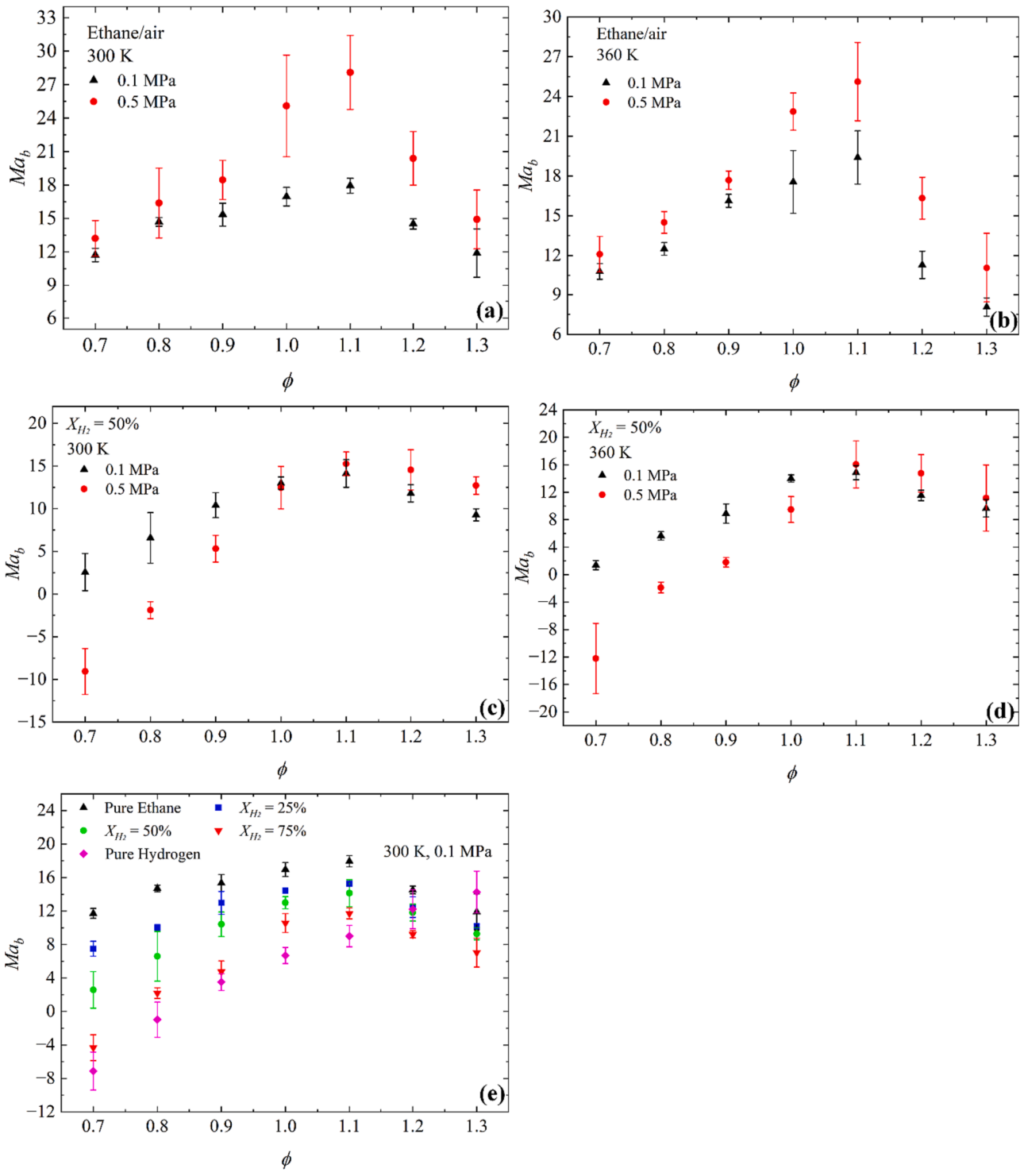

Fig. 10. The variations of measured burned gas Markstein number, Ma_b, of ethane/hydrogen/air mixtures with equivalence ratio, ϕ, at conditions initial temperature of 300, 360 K, and initial pressure of 0.1, 0.5 MPa.

generally decreases with an equivalence ratio from 0.7 to 1.1, and increases from 1.1 to 1.3 under all conditions and mixtures. An increase in temperature results in a slight thickening of the flame, while an increase in pressure significantly reduces the flame thickness several-fold. Incorporating additional hydrogen results in a thinner flame, thereby both increasing in pressure and hydrogen additions amplifying the hydrodynamic instability effects.

In Fig. 8 (c), it is evident that the thermal expansion coefficient is notably sensitive to temperature variations. As the temperature increases, the thermal expansion coefficient correspondingly decreases. Concurrently, when there is a rise in pressure, the coefficient experiences a slight increase. Furthermore, Fig. 8 (d) illustrates that an increase in hydrogen content tends to diminish the coefficient as well. From Fig. 8 (e), it is noticed that pressure, temperature and equivalence ratio have negligible effects on the effective Lewis number, Le_{eff}, while an increase in hydrogen addition leads to its decrease. The Le_{eff} values are observed to be larger than unity in conditions of pure ethane andX_{H_2} = 25 %. As X_{H_2} increases to 50 %, 75 % and 100 %, the values of Le_{eff}

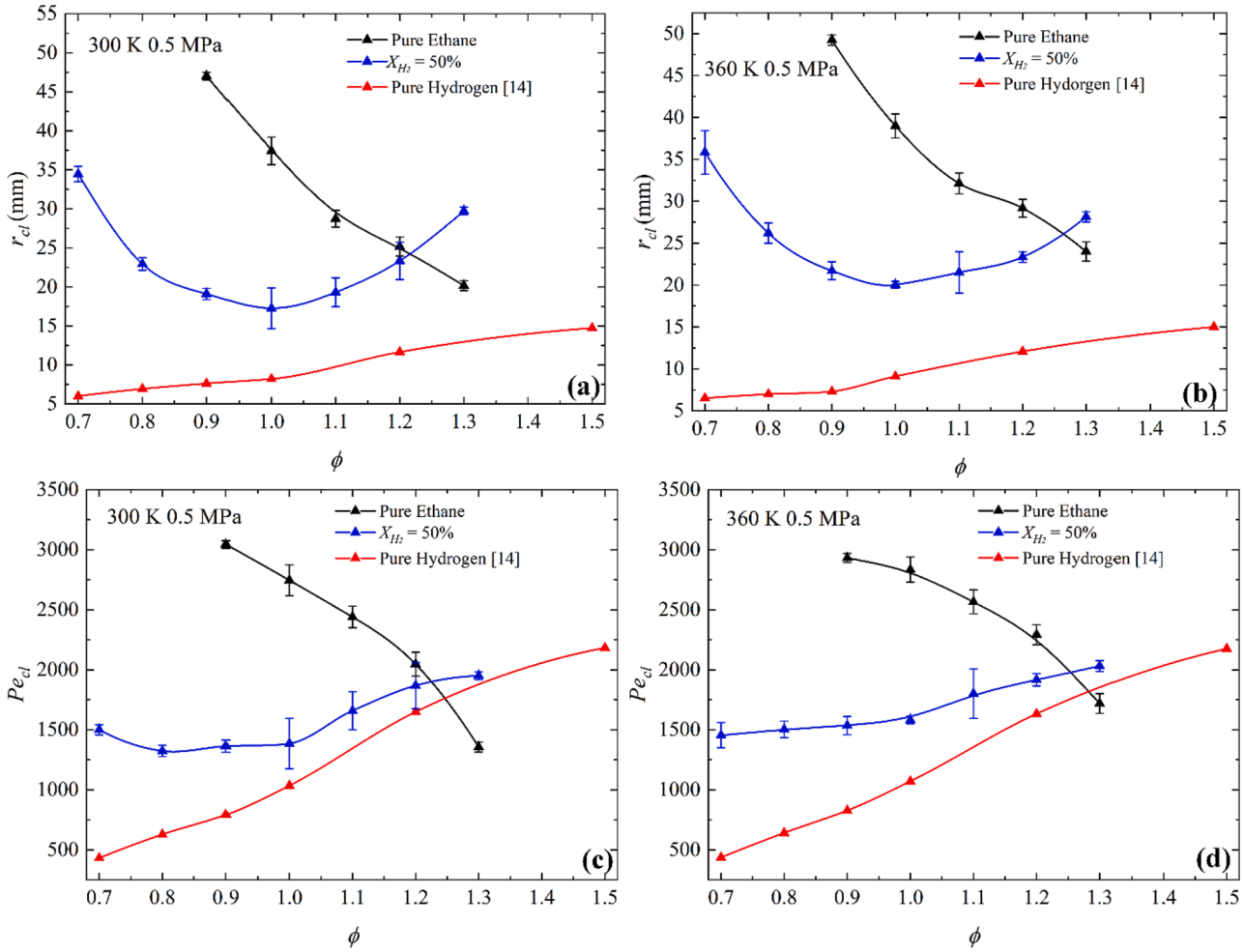

Fig. 11. The variations of measured Peclet number, Pe_{cl}, and critical radius, r_{cl}, of ethane/hydrogen/air mixtures with equivalence ratio, ϕ, at conditions initial temperature of 300, 360 K, and pressure of 0.5 MPa.

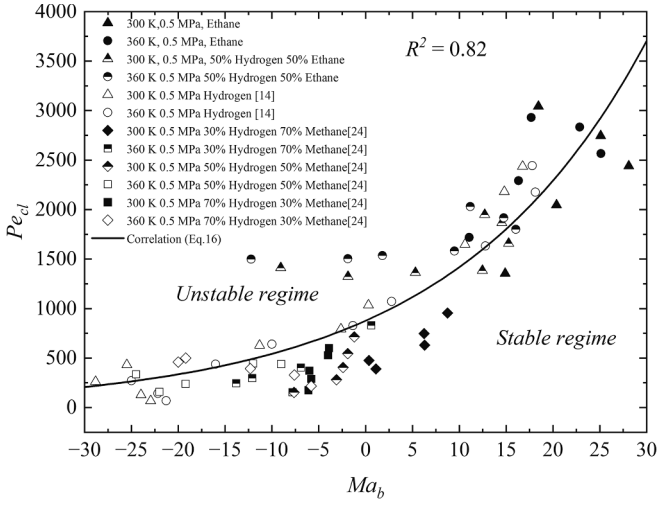

Fig. 12. Variations of Pe_{cl} with Ma_b for ethane/air, ethane/hydrogen/air (X_{H_2} = 50 %), methane/hydrogen/air (X_{H_2} = 30 %, 50 % and 70 %) from [24] and hydrogen/air from [14] at 0.5 MPa. The solid curve represents the correlation (Eq. (16).

Table A1
Experimental data of ethane/air at 300 K, 0.1 MPa.

ϕ	ρ_u/ρ_b	Ss (m/s)	u_l (m/ s)	δ_l(mm)	L_b (mm)	Ma_b	Le
0.7	6.371	1.469 ± 0.06	0.231 ± 0.01	0.0829	0.972 ± 0.05	11.7 ± 0.6	1.466
0.8	6.946	2.063 ± 0.04	0.297 ± 0.006	0.0640	0.941 ± 0.02	14.7 ± 0.4	1.458
0.9	7.450	2.714 ± 0.06	0.364 ± 0.008	0.0516	0.792 ± 0.05	15.3 ± 1.0	1.450
1.0	7.817	3.140 ± 0.08	0.402 ± 0.01	0.0466	0.802 ± 0.04	16.9 ± 0.8	1.443
1.1	7.922	3.274 ± 0.07	0.413 ± 0.009	0.0450	0.807 ± 0.03	17.9 ± 0.7	1.436
1.2	7.841	3.097 ± 0.05	0.395 ± 0.007	0.0468	0.679 ± 0.02	14.5 ± 0.5	1.429
1.3	7.718	2.634 ± 0.06	0.341 ± 0.008	0.0539	0.641 ± 0.12	11.9 ± 2.2	1.425

transition to less than unity. This trend indicates a strengthening in the effects of thermal-diffusivity instability concurrent with the rise in X_{H_2}. Notably, for the cases whereX_{H_2} = 50 %, Le_{eff} approaches near unity, symbolizing a near absence of thermal-diffusivity instability effects.

3.6. Markstein length and number

The burned gas Markstein length, L_b, of ethane/hydrogen/air mix-

Table A2
Experimental data of ethane/air at 360 K, 0.1 MPa.

ϕ	ρ_u/ρ_b	Ss (m/s)	u_l (m/ s)	δ_l(mm)	L_b (mm)	Ma_b	Le
0.7	5.431	1.651 ± 0.06	0.304 ± 0.011	0.0865	0.934 ± 0.05	10.8 ± 0.6	1.436
0.8	5.902	2.250 ± 0.05	0.381 ± 0.009	0.0684	0.856 ± 0.03	12.5 ± 0.5	1.428
0.9	6.308	2.986 ± 0.08	0.473 ± 0.012	0.0547	0.882 ± 0.03	16.1 ± 0.5	1.420
1.0	6.606	3.534 ± 0.06	0.535 ± 0.009	0.0482	0.846 ± 0.08	17.6 ± 2.4	1.413
1.1	6.702	3.684 ± 0.05	0.550 ± 0.008	0.0466	0.904 ± 0.06	19.4 ± 2.0	1.406
1.2	6.649	3.549 ± 0.05	0.534 ± 0.008	0.0476	0.538 ± 0.05	11.3 ± 1.0	1.400
1.3	6.554	3.240 ± 0.05	0.494 ± 0.008	0.0512	0.412 ± 0.04	8.1 ± 0.7	1.395

tures were measured and presented in Fig. 9 at the initial temperature 300–360 K, pressure 0.1–0.5 MPa, with hydrogen addition X_{H_2} = 0 %, 25 %, 50 %, 75 % and 100 %. The burned gas Markstein length, L_b represents the effect of stretch rate on the flame speeds, the positive value of L_b indicating the decreasing of stretch rate accelerate the flame speed and negative value of L_b has reverse effect. As shown in Fig. 9 from (a) to (d), for both X_{H_2} = 0 % and 50 %, the L_b decreases as pressure increase indicating the influence of stretch rate on the flame speed declining at high pressure. This general declining effect is consisting with the experimental work of Zuo et al. [12] for ethane/air and other hydrocarbons including methane/air [12,24,27], propane/air [12] and *i*-octane/*n*-heptane/air [34] mixtures. While, increasing temperature from 300 K to 360 K, the L_b only reduces slightly, meanwhile, L_b keeps decreasing as mixture becomes richer for pure ethane indicating the decaying effects of stretch rate on burning velocity. Shown in Fig. 9 (e), compared with pure ethane/air mixture, hydrogen tends to reverse the trend of L_b with equivalence ratio and negative L_b observed at $\phi = 0.7$ withX_{H_2} = 75 % and 100 % showing that the stretch rate has negative effects on the flame speed. Moreover, the additions of hydrogen lead to the decreases of L_b with the same equivalence ratio indicating the decaying effects of stretch rate on flame speed of the ethane/hydrogen/air mixtures.

Bechtold and Matalon [52] have provided an expression for the Markstein length through asymptotic analysis to explain the factors that influence it, as shown in Eq. (15) below:

$$L_b = \delta_l\{\frac{2}{\sqrt{\sigma}+1} + \frac{2Ze\left(Le_{eff}-1\right)}{\sigma-1}[\sqrt{\sigma}-1-ln\frac{\sqrt{\sigma}-1}{2}]\} \quad (15)$$

where, Ze is the Zel'dovich number. In this study, the value of δ_l, Ze, Le_{eff}, σ and the term $[\sqrt{\sigma}-1-ln\frac{\sqrt{\sigma}-1}{2}]$ are all positive. Thus, the term $\left(Le_{eff}-1\right)$ fundamentally dictates the positivity or negativity of L_b. If L_b

Table A5
Experimental data of ethane/hydrogen/air (X_{H_2} = 50 %) at 300 K, 0.1 MPa.

ϕ	ρ_u/ρ_b	Ss (m/s)	u_l (m/ s)	δ_l(mm)	L_b (mm)	Ma_b	Le_{eff}
0.7	6.316	1.842 ± 0.06	0.292 ± 0.009	0.0741	0.190 ± 0.10	2.6 ± 2.2	0.933
0.8	6.863	2.741 ± 0.1	0.399 ± 0.014	0.0546	0.359 ± 0.11	6.6 ± 3.0	0.933
0.9	7.326	3.407 ± 0.04	0.465 ± 0.006	0.0473	0.493 ± 0.07	10.4 ± 1.5	0.933
1.0	7.658	3.980 ± 0.06	0.520 ± 0.008	0.0427	0.555 ± 0.03	13.0 ± 0.7	0.932
1.1	7.751	4.315 ± 0.06	0.557 ± 0.008	0.0402	0.568 ± 0.07	14.1 ± 1.6	0.931
1.2	7.673	4.087 ± 0.05	0.533 ± 0.006	0.0424	0.501 ± 0.04	11.8 ± 1.0	0.930
1.3	7.555	3.544 ± 0.07	0.469 ± 0.009	0.0486	0.451 ± 0.03	9.3 ± 0.7	0.929

Table A6
Experimental data of ethane/hydrogen/air (X_{H_2} = 50 %) at 360 K, 0.1 MPa.

ϕ	ρ_u/ρ_b	Ss (m/s)	u_l (m/ s)	δ_l(mm)	L_b (mm)	Ma_b	Le_{eff}
0.7	5.401	2.036 ± 0.03	0.377 ± 0.006	0.0788	0.108 ± 0.04	1.4 ± 0.7	0.917
0.8	5.823	3.018 ± 0.07	0.518 ± 0.012	0.0577	0.326 ± 0.03	5.7 ± 0.6	0.916
0.9	6.203	3.796 ± 0.05	0.612 ± 0.008	0.0493	0.438 ± 0.07	8.9 ± 1.4	0.916
1.0	6.468	4.547 ± 0.08	0.703 ± 0.013	0.0432	0.605 ± 0.05	14.0 ± 0.5	0.915
1.1	6.556	4.668 ± 0.06	0.712 ± 0.009	0.0431	0.640 ± 0.04	14.9 ± 1.0	0.914
1.2	6.507	4.548 ± 0.09	0.699 ± 0.014	0.0442	0.510 ± 0.03	11.5 ± 0.8	0.912
1.3	6.415	3.918 ± 0.12	0.611 ± 0.019	0.0509	0.422 ± 0.06	9.7 ± 1.3	0.911

Table A3
Experimental data of ethane/air at 300 K, 0.5 MPa.

ϕ	ρ_u/ρ_b	Ss (m/s)	u_l (m/s)	δ_l(mm)	L_b (mm)	Ma_b	r_{cl} (mm)	Pe_{cl}	Le
0.7	6.378	0.774 ± 0.06	0.121 ± 0.009	0.0314	0.415 ± 0.05	13.2 ± 1.6	–	–	1.464
0.8	6.965	1.282 ± 0.06	0.184 ± 0.008	0.0224	0.337 ± 0.06	16.4 ± 3.1	–	–	1.456
0.9	7.505	1.831 ± 0.06	0.244 ± 0.008	0.0155	0.285 ± 0.03	18.5 ± 1.8	47 ± 0.5	3040 ± 32	1.449
1.0	7.922	2.179 ± 0.1	0.275 ± 0.013	0.0136	0.342 ± 0.06	25.1 ± 4.6	37.4 ± 1.8	2750 ± 129	1.442
1.1	7.977	2.526 ± 0.07	0.317 ± 0.009	0.0118	0.331 ± 0.04	28.1 ± 3.3	28.7 ± 1.1	2440 ± 90	1.434
1.2	7.863	2.372 ± 0.07	0.302 ± 0.009	0.0123	0.251 ± 0.03	20.4 ± 2.4	25.2 ± 1.2	2050 ± 100	1.427
1.3	7.729	1.912 ± 0.06	0.247 ± 0.008	0.0149	0.222 ± 0.04	14.9 ± 2.6	20.2 ± 0.6	1360 ± 42	1.420

Table A4
Experimental data of ethane/air at 360 K, 0.5 MPa.

ϕ	ρ_u/ρ_b	Ss (m/s)	u_l (m/s)	δ_l(mm)	L_b (mm)	Ma_b	r_{cl} (mm)	Pe_{cl}	Le
0.7	5.438	0.910 ± 0.04	0.167 ± 0.008	0.0314	0.380 ± 0.04	12.1 ± 1.3	–	–	1.435
0.8	5.922	1.378 ± 0.04	0.233 ± 0.008	0.0224	0.325 ± 0.02	14.5 ± 0.8	–	–	1.427
0.9	6.362	1.961 ± 0.05	0.308 ± 0.008	0.0168	0.297 ± 0.02	17.7 ± 0.7	49.2 ± 0.6	2930 ± 37	1.419
1.0	6.697	2.507 ± 0.06	0.374 ± 0.009	0.0138	0.315 ± 0.02	22.9 ± 1.4	39.0 ± 1.4	2830 ± 104	1.412
1.1	6.759	2.762 ± 0.03	0.409 ± 0.005	0.0125	0.315 ± 0.04	25.1 ± 2.9	32.1 ± 1.2	2560 ± 100	1.405
1.2	6.674	2.669 ± 0.05	0.401 ± 0.007	0.0127	0.208 ± 0.02	16.3 ± 1.6	29.2 ± 1.1	2290 ± 83	1.398
1.3	6.567	2.379 ± 0.05	0.362 ± 0.007	0.0141	0.155 ± 0.04	11.1 ± 2.6	24.0 ± 1.1	1720 ± 82	1.391

Table A7
Experimental data of ethane/hydrogen/air (X_{H_2} = 50 %) at 300 K, 0.5 MPa.

ϕ	ρ_u/ρ_b	Ss (m/s)	u_l (m/s)	δ_l(mm)	L_b (mm)	Ma_b	r_{cl} (mm)	Pe_{cl}	Le_{eff}
0.7	6.323	1.190 ± 0.05	0.188 ± 0.008	0.0230	−0.209 ± 0.06	−9.1 ± 2.7	34.5 ± 1.0	1413 ± 43	0.932
0.8	6.874	1.730 ± 0.06	0.252 ± 0.009	0.0173	−0.033 ± 0.02	−1.9 ± 1.0	22.9 ± 0.8	1323 ± 46	0.933
0.9	7.374	2.328 ± 0.07	0.316 ± 0.01	0.0139	0.074 ± 0.02	5.3 ± 1.6	19.1 ± 0.7	1363 ± 51	0.932
1.0	7.763	2.771 ± 0.05	0.357 ± 0.006	0.0125	0.155 ± 0.03	12.5 ± 2.5	17.3 ± 2.6	1385 ± 210	0.931
1.1	7.810	3.012 ± 0.04	0.386 ± 0.005	0.0116	0.178 ± 0.02	15. 3 ± 1.4	19.3 ± 1.8	1659 ± 159	0.930
1.2	7.698	2.789 ± 0.1	0.362 ± 0.013	0.0125	0.182 ± 0.03	14.5 ± 2.4	23.3 ± 2.4	1867 ± 192	0.928
1.3	7.570	2.263 ±0.08	0.299 ± 0.011	0.0153	0.194 ± 0.03	12.7 ± 1.0	29.7 ± 0.5	1950 ± 33	0.927

Table A8
Experimental data of ethane/hydrogen/air (X_{H2} = 50 %) at 360 K, 0.5 MPa.

ϕ	ρ_u/ρ_b	Ss (m/s)	u_l (m/s)	δ_l(mm)	L_b (mm)	Ma_b	r_{cl} (mm)	Pe_{cl}	Le_{eff}
0.7	5.390	1.297 ± 0.04	0.241 ± 0.008	0.0246	−0.301 ± 0.11	−12 ± 5.1	35.8 ± 2.6	1450 ± 106	0.917
0.8	5.844	2.0041 ± 0.05	0.343 ± 0.009	0.0174	−0.033 ± 0.03	−1.9 ± 0.8	26.2 ± 1.2	1502 ± 69	0.916
0.9	6.251	2.667 ± 0.07	0.427 ± 0.011	0.0141	0.025 ± 0.06	1.8 ± 0.7	21.7 ± 1.1	1535 ± 76	0.915
1.0	6.563	3.157 ± 0.05	0.481 ± 0.008	0.0127	0.120 ± 0.02	9.5 ± 1.9	20.0 ± 0.4	1582 ± 32	0.914
1.1	6.617	3.403 ± 0.06	0.514 ± 0.009	0.0119	0.192 ± 0.04	16.1 ± 3.4	21.5 ± 2.5	1801 ± 206	0.913
1.2	6.534	3.322 ± 0.06	0.508 ± 0.009	0.0122	0.180 ± 0.03	14.8 ± 2.7	23.3 ± 0.6	1916 ± 51	0.911
1.3	6.431	2.896 ± 0.08	0.450 ± 0.012	0.0139	0.155 ± 0.07	11.2 ± 4.8	28.1 ± 0.6	2030 ± 45	0.909

Table A9
Experimental data of ethane/hydrogen/air (X_{H_2} = 25 %) at 300 K, 0.1 MPa.

ϕ	ρ_u/ρ_b	Ss (m/s)	u_l (m/s)	δ_l(mm)	L_b (mm)	Ma_b	Le_{eff}
0.7	6.335	1.493 ± 0.06	0.236 ± 0.009	0.0811	0.683 ± 0.08	7.5 ± 0.9	1.199
0.8	6.929	2.155 ± 0.05	0.311 ± 0.007	0.0629	0.699 ± 0.02	10.0 ± 0.3	1.195
0.9	7.400	2.829 ± 0.06	0.382 ± 0.008	0.0503	0.743 ± 0.08	13.0 ± 1.4	1.191
1.0	7.763	3.366 ± 0.07	0.434 ± 0.009	0.045	0.736 ± 0.01	14.4 ± 0.1	1.187
1.1	7.855	3.564 ± 0.06	0.454 ± 0.008	0.0431	0.746 ± 0.01	15.2 ± 0.2	1.183
1.2	7.773	3.412 ± 0.09	0.439 ± 0.011	0.0456	0.639 ± 0.06	12.5 ± 1.2	1.180
1.3	7.656	2.909 ± 0.08	0.380 ± 0.01	0.0529	0.605 ± 0.02	10.2 ± 0.3	1.177

Table A10
Experimental data of ethane/hydrogen/air (X_{H_2} = 75 %) at 300 K, 0.1 MPa.

ϕ	ρ_u/ρ_b	Ss (m/s)	u_l (m/s)	δ_l(mm)	L_b (mm)	Ma_b	Le_{eff}
0.7	6.190	2.592 ± 0.04	0.419 ± 0.007	0.0664	−0.287 ± 0.1	−4.3 ± 1.5	0.667
0.8	6.767	3.900 ± 0.07	0.576 ± 0.011	0.0498	0.109 ± 0.03	2.2 ± 0.6	0.671
0.9	7.151	4.782 ± 0.08	0.669 ±0.012	0.0444	0.211 ± 0.06	4.7 ± 1.3	0.674
1.0	7.456	5.630 ± 0.1	0.755 ± 0.014	0.0404	0.426 ± 0.05	10.6 ± 1.1	0.677
1.1	7.531	5.940 ± 0.06	0.789 ± 0.008	0.0397	0.465 ± 0.03	11.7 ± 0.6	0.678
1.2	7.453	5.736 ± 0.09	0.770 ± 0.012	0.0418	0.386 ± 0.02	9.2 ± 0.4	0.680
1.3	7.343	5.132 ± 0.07	0.699 ± 0.01	0.0472	0.332 ± 0.08	7.0 ± 1.7	0.681

Table A11
Experimental data of hydrogen/air at 300 K, 0.1 MPa.

ϕ	ρ_u/ρ_b	Ss (m/s)	u_l (m/s)	δ_l(mm)	L_b (mm)	Ma_b	Le
0.7	5.981	8.592 ± 0.33	1.437 ± 0.055	0.0441	−0.314 ± 0.1	−7.1 ± 2.3	0.401
0.8	6.361	11.484 ± 0.18	1.805 ± 0.028	0.0357	−0.035 ± 0.08	−1.0 ± 2.1	0.409
0.9	6.666	13.736 ± 0.17	2.061 ± 0.026	0.0341	0.119 ± 0.03	3.5 ± 1.0	0.416
1.0	6.863	15.272 ± 0.19	2.225 ± 0.028	0.0301	0.201 ± 0.03	6.7 ± 1.0	0.421
1.1	6.893	16.899 ± 0.19	2.452 ± 0.028	0.0291	0.261 ± 0.04	9.0 ± 1.3	0.426
1.2	6.824	18.028 ± 0.27	2.642 ± 0.04	0.0283	0.346 ± 0.07	12.2 ± 2.3	0.430
1.3	6.733	18.699 ± 0.22	2.777 ± 0.033	0.0272	0.385 ± 0.07	14.3 ± 2.5	0.433

is negative, $Le_{eff} < 1$, representing the flame is under the effects of thermal-diffusive instability. Conversely, L_b is positive yields $Le_{eff} > 1$, representing a stable propagation flame. Eq. (15) reveal that the δ_l predominantly controls the magnitude of L_b, clarifying that an increasing in pressure results in a diminished flame thickness and subsequently, a reduced magnitude of L_b.

The measured burned gas Markstein number, Ma_b, at the same conditions as Fig. 9 is illustrated in Fig. 10. The Ma_b is a dimensionless parameter equaling to L_b divided the flame thickness, δ_l. This parameter characterizes the cumulative effect of the stretch rate on the expanding flame surface. The Ma_b serves as a dimensionless unit, correlated with another dimensionless parameter, the Peclet number, Pe_{cl} to define the stable and unstable regime of expanding flame [16,24,53,54]. In general, similar to L_b, the value of Ma_b decreases with increasing pressure and X_{H_2}. The Ma_b initially increases from lean to stoichiometric conditions, then decreases towards the rich side for X_{H_2} = 0 % − 75 %. For pure hydrogen cases (X_{H_2} = 100 %), Ma_b continuously increases with the equivalence ratio, transitioning from a negative value in lean mixtures to a positive value in rich mixtures. Moreover, when compared with hydrogen/air, the ethane/air has bigger Ma_b indicating the flame speed is more sensitive to the stretch rate.

3.7. Instability parameters, r_{cl} and Pe_{cl}

The critical radius, r_{cl}, is an important parameter to characterize the cellular instability of expanding premixed laminar flame. As illustrated in Fig. 3, for the case at 300 K, 0.5 MPa, this critical radius is identified at the onset of cellular instability. This is where the flame speed undergoes a significant increase in relation to the stretch rate. The cellular nature of the flame surface arises due to the influences of hydrodynamic and thermal-diffusivity instabilities. The cellular instability arises due to an increase in the stretched flame front area, enhancing the combustion

volume rate, while the effects of chemical kinetics remain unchanged. within the current measurement ranges (r_{sch} < 60 mm), at 0.1 MPa conditions, no cellular instability was observed for the ethane/air mixture. This is attributed to$Le_{eff} > 1$, where thermal diffusivity stabilizes the flame, and the impact of hydrodynamic instability is diminished due to the relatively thick flame thickness. Compared with the ethane/air, and referring to Fig. 8 (b) for flame thickness and Fig. 8 (e) for Le_{eff} at 0.1 MPa, an increase in X_{H_2} results in a decrease in flame thickness and Le_{eff} and this amplifies the effects of both hydrodynamic and thermal-diffusivity instability. This explained the cellular instability occurs for hydrogen/air mixtures even at 0.1 MPa.

Fig. 11 (a)&(b) show the critical radius at temperature of 300 and 360 K, pressure 0.5 MPa with ethane/air, X_{H_2} = 50 % and pure hydrogen from [14]. The r_{cl} is not sensitivity to the temperature changes when it rises from 300 K to 360 K, for all three types of mixtures. For ethane/air mixtures, cellular instability at 0.5 MPa is dominated by the hydrodynamic instability, the critical radius starts from 46 mm for mixture with $\phi = 0.9$, and gradually decreases with ϕ indicates that the cellular instability occurs earlier for rich mixtures. While, for the hydrogen/air mixture at 0.5 MPa, both hydrodynamic and thermal-diffusivity instability ($Le_{eff} \ll 1$) dominate the cellular instability the critical radius of hydrogen/air mixture gradually increases with the ϕ indicating the lean hydrogen/air flames are prone to combustion instabilities. For $X_{H_2} = 50$ %, the effects of thermal-diffusivity instability can be neglected because $Le_{eff} \approx 1$, resulting in the dominance of hydrodynamic instability. From lean to stochiometric, the r_{cl} decreases with ϕ, indicating an enhancement of hydrodynamic instability due to a decrease in flame thickness and an increase in thermal expansion coefficient, as shown in Fig. 8 (a) and (c). However, moving from stochiometric to rich conditions, r_{cl} increases with ϕ, signifying a weakening of hydrodynamic instability as the flame thickness increases and the thermal expansion coefficient decreases.

The critical Peclet number, Pe_{cl}, is determined by normalizing r_{cl} with δ_l, characterizing the onset of flame cellularity due to both hydrodynamic and thermal-diffusivity instabilities. This dimensionless parameter is plotting against ϕ in Fig. 11 (c)&(d) following a trend similar to r_{cl}. Numerous researchers have posited that cellular instability is linked to the effects of stretch rate, and have correlated Pe_{cl} with Ma_b to define the stable and unstable regime of expanding flame [14,16,24,53,54]. Xie et al. [14], Kim et al. [53] and Mohamed [16] correlated the Pe_{cl} with Ma_b to defined the stable regime of hydrogen/air mixture covering a wild range of equivalence ratio, pressure and temperature. For hydrocarbon fuels, Oppong et al. [54] proposed correlation for ethyl acetate/air over a wide range of temperature from 358 K to 418 K. Marwaan et al [24], measured both Pe_{cl} and Ma_b for methane/hydrogen/air mixtures with pressure up to 1 MPa. However, a knowledge gap persists concerning the boundary of the stable regime for ethane/hydrogen/air mixtures. It is therefore valuable to amalgamate data from existing literature with current measurements to propose a general correlation applicable to various fuels.

The Pe_{cl} with Ma_b values for ethane/air and ethane/hydrogen/air mixtures ($X_{H_2} = 50$ %) from the current study, along with data from Xie et al. [14] on hydrogen/air and Marwaan et al [24] on methane/hydrogen/air ($X_{H_2} = 30$ %, 50 % and 70 %) covering a wide range of equivalence ratio, temperature and pressure at 0.5 MPa are collectively presented with symbols in Fig. 12. Following the correlation format used in [14,27,55], a non-linear correlation is purposed to best fit the measurement, aiding in the identification of the stable and unstable flame regimes:

$$Pe_{cl} = 877exp(0.04803Ma_b),\ Mab \in (-30\,30) \tag{16}$$

The solid curve in Fig. 12 represents this non-linear correlation, exhibiting an R^2 value of 0.82, demonstrating a good fit with the measured data. The stable regime is located below the curve, while the unstable regime is situated above it. Overall, the results illustrate that Pe_{cl} increases with Ma_b implying that the flames become more stable with increasing Ma_b. The hydrogen/air, methane/hydrogen/air (X_{H_2} = 30 %, 70 % and 50 %) and lean ethane/hydrogen/air ($X_{H_2} = 50$ %) are mixtures are characterized by negative Ma_b and minimal Pe_{cl}. This suggests that cellular instability occurs early with small flame radius and a limited stable flame propagation regime. Noted, in comparison to hydrogen/air mixtures, ethane/hydrogen/air (X_{H_2} = 50 %) exhibit positive Ma_b and large Pe_{cl} demonstrating that adding ethane to hydrogen reduces the inherent cellular instability, expanding the stable regime relative to pure hydrogen. In ethane/air mixtures, strong positive Ma_b, values are prominent, leading to a more stable flame and cellular instability only occurring at large Pe_{cl} and radius. When compared to methane/hydrogen/air mixtures at the same hydrogen level of$X_{H_2} = 50$ % ethane/hydrogen/air mixtures exhibit superior resistance to cellular instability, displaying relatively larger Ma_b and Pe_{cl} values.

4. Conclusion

The laminar burning velocities of spherical propagating ethane/hydrogen/air premixed flames were measured in a spherical constant-volume combustion vessel. The effects of various temperature (300 K − 360 K), pressure (0.1 MPa − 0.5 MPa), equivalence ratio (ϕ = 0.7—1.3) and hydrogen ratio ($X_{H_2} = 0$ % − 100 %) were examined in detail. Key combustion characteristics such Markstein length/number, flame thickness, effective Lewis number, thermal expansion coefficient and critical conditions at the onset of cellular instability including critical radius and Peclet number, were either measured or calculated. The laminar burning velocity increases with increasing X_{H_2} due to the enhancement of both thermal and chemical kinetics effects. The current measurements of the laminar burning velocity of ethane/air are in good agreement with those of Lowry et al. [7] at 0.1, 0.5 MPa and 300 K and with Goswami et al. [10] at 0.1 MPa.

Predictions of the laminar burning velocity from the chemical kinetics mechanisms, Aramco Mech 1.3 [28] and USC Mech II [31] showed agreement with measurements under specific initial conditions. However, both mechanisms overpredicted the laminar burning velocity at an initial temperature of 360 K. The dependence of the ethane/hydrogen/air laminar burning velocities on temperature, pressure, and hydrogen ratio was analyzed using a datum empirical expression and blending law, yielding excellent agreement. The measured Markstein length of ethane/hydrogen/air decreases with the increasing pressure and X_{H_2} primarily due to reductions in flame thickness and effective Lewis number, amplifying the effects of hydrodynamic and thermal-diffusivity instability. Cellular instability, predominated by hydrodynamic instabilities, was observed at 0.5 MPa for ethane/air and ethane/hydrogen/air ($X_{H_2} = 50$ %).

A general correlation was proposed, based on the Peclet number against with the Markstein number, for various mixtures including hydrogen/air, ethane/hydrogen/air (X_{H_2} = 0 % and 50 %) and methane/hydrogen/air ($X_{H_2} = 30$ %, 50 % and 70 %). This correlation, covering a wide range of equivalence ratios, temperatures, and pressures at 0.5 MPa, aims to define the stable and unstable regimes of flame propagation. It exhibits an R^2 value of 0.82, demonstrating a strong fit with the measured data. When compared with methane at the identical X_{H_2} level, ethane displays superior resistance to cellular instability. The introduction of ethane into hydrogen appears promising in mitigating the effects of cellular flame instability, thereby fostering stable flame propagation.

5. Novelty and significance

The present research contributes to the understanding of laminar flame characteristics of ethane/hydrogen/air mixtures across a wide range of conditions. The Leeds fan-stirred constant volume combustion vessel has been utilized to measure key combustion parameters, such as

laminar burning velocity, Markstein length, and critical conditions signaling the onset of cellular instability, including critical radius and Peclet number. The measured laminar burning velocities are compared with the predictions from chemical kinetic mechanisms, revealing that these predictions are consistently overestimated at a temperature of 360 K. A general correlation has been established, relating the Peclet number to the Markstein number, for a variety of mixtures and conditions. This correlation aids in discerning stable from unstable flame propagation regimes, indicating that a higher Markstein number tends to stabilize flame propagation.

CRediT authorship contribution statement

Jinzhou Li: Writing – original draft, Visualization, Validation, Methodology, Investigation, Formal analysis, Data curation. **Yu Xie:** Visualization, Validation, Methodology. **Mohamed Elsayed Morsy:** Writing – review & editing, Methodology. **Junfeng Yang:** Writing – review & editing, Supervision, Resources, Project administration, Funding acquisition, Conceptualization.

Declaration of competing interest

The authors declare that they have no known competing financial interests or personal relationships that could have appeared to influence the work reported in this paper.

Data availability

Data will be made available on request.

Acknowledgments

Thanks are given to EPSRC (Grant No. EP/W002299/1) for financial support. Mr. Jinzhou Li acknowledges the Shell Global Solution Ltd. (UK) for providing the partial financial support on the PhD project.

Appendix

(See Table A1 –A11).

References

[1] National Grid ESO, Britain's Electricity Explained: 2022 Review, https://www.nationalgrideso.com/news/britains-electricity-explained-2022-review. 2023.
[2] Liss WR, Thrasher WH, Steinmetz GF, Chowdiah P, Attari A. Variability of Natural Gas Composition in Select Major Metropolitan Areas of the United States. American Gas Association Laboratories, Cleveland, OH: Final Report; 1992.
[3] Young J. U.S. ethane production established a new record in April 2023. US Energy Information Administration 2023.
[4] Szwaja S, Kovacs VB, Bereczky A, Penninger A. Sewage sludge producer gas enriched with methane as a fuel to a spark ignited engine. Fuel Process Technol 2013;110:160–6.
[5] Wei H, Zhang R, Chen L, Pan J, Wang X. Effects of high ignition energy on lean combustion characteristics of natural gas using an optical engine with a high compression ratio. Energy 2021;223:120053.
[6] Nilsson EJ, van Sprang A, Larfeldt J, Konnov AA. Effect of natural gas composition on the laminar burning velocities at elevated temperatures. Fuel 2019;253:904–9.
[7] Lowry W, de Vries J, Krejci M, Petersen E, Serinyel Z, Metcalfe W, et al. Laminar flame speed measurements and modeling of pure alkanes and alkane blends at elevated pressures. J Eng Gas Turbines Power 2011;133:9.
[8] Mitu M, Razus D, Giurcan V, Oancea D. Normal burning velocity and propagation speed of ethane-air: Pressure and temperature dependence. Fuel 2015;147:27–34.
[9] Nilsson EJ, Van Sprang A, Larfeldt J, Konnov AA. The comparative and combined effects of hydrogen addition on the laminar burning velocities of methane and its blends with ethane and propane. Fuel 2017;189:369–76.
[10] Goswami M, Bastiaans RJM, De Goey LPH, Konnov AA. Experimental and modelling study of the effect of elevated pressure on ethane and propane flames. Fuel 2016;166:410–8.
[11] Ravi S, Sikes TG, Morones A, Keesee CL, Petersen EL. Comparative study on the laminar flame speed enhancement of methane with ethane and ethylene addition. Proc Combust Inst 2015;35:679–86.
[12] Zuo Z, Hu B, Bao X, Zhang S, Fan L, Deng L, et al. Self-acceleration characteristics of premixed C1–C3 alkanes-air mixtures in a constant-volume chamber. Fuel Process Technol 2022;231:107252.
[13] Zuo Z, Hu B, Bao X, Zhang S, Kong L, Deng L, et al. Quantitative research on cellular instabilities of premixed C1–C3 alkane–air mixtures using spherically expanding flames. Fuel Process Technol 2022;226:107075.
[14] Xie Y, Morsy ME, Li J, Yang J. Intrinsic cellular instabilities of hydrogen laminar outwardly propagating spherical flames. Fuel 2022;327:125149.
[15] Bradley D, Lawes M, Liu K, Verhelst S, Woolley R. Woolley, Laminar burning velocities of lean hydrogen-air mixtures at pressures up to 1.0 MPa. Combust. Flame 2007;149:162–72.
[16] Morsy ME, Yang J. The instability of laminar methane/hydrogen/air flames: Correlation between small and large-scale explosions. Int J Hydrogen Energy 2022;47:29959–70.
[17] Liu Q, Chen X, Shen Y, Zhang Y. Parameter extraction from spherically expanding flames propagated in hydrogen/air mixtures. Int J Hydrogen Energy 2019;44:1227–38.
[18] Sierens R, Rosseel E. Variable composition hydrogen/natural gas mixtures for increased engine efficiency and decreased emissions. J Eng Gas Turbines Power 2000;122:135–40.
[19] Bennister RL, Newby RA, Yang W. Final report on the development of a hydrogen-fueled combustion gas turbine cycle for power generation. J Eng Gas Turbines Power 1999;121:38–45.
[20] Bell SR, Gupta M. Extension of the lean operating limit for natural gas fueling of a spark ignited engine using hydrogen blending. Combust Sci Technol 1997;123:23–48.
[21] Natkin RJ, Tang X, Boyer B, Otmans B, Denlinger A, Heffel JW. Hydrogen IC engine boosting performance and NOx study. SAE Trans 2003;865–875.
[22] Law CK, Kwon OC. Effects of hydrocarbon substitution on atmospheric hydrogen-air flame propagation. Int J Hydrogen Energy 2004;29:867–79.
[23] Law CK, Jomaas G, Bechtold JK. Cellular instabilities of expanding hydrogen/propane spherical flames at elevated pressures: theory and experiment. Proc Combust Inst 2005;30:159–67.
[24] Marwaan AK, Yang J, Tomlin AS, Thompson HM, de Boer G, Liu K, et al. Laminar burning velocities and Markstein numbers for pure hydrogen and methane/hydrogen/air mixtures at elevated pressures. Fuel 2023;354:129331.
[25] Li H, Xiao H, Sun J. Laminar burning velocity, Markstein length, and cellular instability of spherically propagating NH3/H2/Air premixed flames at moderate pressures. Combust Flame 2022;241:112079.
[26] Bradley D, Gaskell PH, Gu XJ. Burning velocities, Markstein lengths, and flame quenching for spherical methane-air flames: a computational study. Combust Flame 1996;104:176–98.
[27] Gu XJ, Haq MZ, Lawes M, Woolley R. Laminar burning velocity and Markstein lengths of methane-air mixtures. Combust Flame 2000;121:41–58.
[28] Metcalfe WK, Burke SM, Ahmed SS, Curran HJ. A hierarchical and comparative kinetic modeling study of C1–C2 hydrocarbon and oxygenated fuels. Int J Chem Kinet 2013;45:638–75.
[29] Smith GP, Golden DM, Frenklach M, Moriarty NW, Eiteneer B, Goldenberg M, Bowman CT, Hanson RK, Song S Gardiner Jr WC, Lissianski VV, Qin Z. GRI-Mech 3.0, http://www.me.berkeley.edu/gri_mech/.
[30] Williams FA, Seshadri K, Catolica R, The San Diego Mechanism, Chemical Kinetic Mechanisms for Combustion Applications. https://web.eng.ucsd.edu/mae/groups/combustion/ mechanism.html. 2015.
[31] Wang H, You X, Joshi AV, Davis SG, Laskin A, Egolfopoulos F, Law CK, USC Mech Version II: high-temperature combustion reaction model of H2/CO/C1-C4 compounds. http://ignis.usc.edu/USC_Mech_II.html. 2007.
[32] MATLAB 2021b, The MathWorks Inc., Natick, Massachusetts, 2021.
[33] Vancoillie J, Sharpe G, Lawes M, Verhelst S. The turbulent burning velocity of methanol-air mixtures. Fuel 2014;130:76–91.
[34] Bradley D, Hicks RA, Lawes M, Sheppard CGW, Woolley R. The measurement of laminar burning velocities and Markstein numbers for iso-octane–air and iso-octane–n-heptane–air mixtures at elevated temperatures and pressures in an explosion bomb. Combust Flame 1998;115:126–44.
[35] C. Morley, GasEq: a chemical equilibrium program for windows, 2005.
[36] Kelley AP, Law CK. Nonlinear effects in the extraction of laminar flame speeds from expanding spherical flames. Combust Flame 2009;156:1844–51.
[37] Bradley D, Sheppard CGW, Woolley R, Greenhalgh DA, Lockett RD. The development and structure of flame instabilities and cellularity at low Markstein numbers in explosions. Combust Flame 2000;122:195–209.
[38] Kwon OC, Rozenchan G, Law CK. Cellular instabilities and self-acceleration of outwardly propagating spherical flames. Proc Combust Inst 2002;29:1775–83.
[39] Okafor EC, Naito Y, Colson S, Ichikawa A, Kudo T, Hayakawa A, et al. Measurement and modelling of the laminar burning velocity of methane-ammonia-air flames at high pressures using a reduced reaction mechanism. Combust Flame 2019;204:162–75.
[40] Bouvet N, Halter F, Chauveau C, Yoon Y. On the effective Lewis number formulations for lean hydrogen/hydrocarbon/air mixtures. Int J Hydrogen Energy 2013;38:5949–60.
[41] Li Y, Bi M, Li B, Zhou Y, Huang L, Gao W. Explosion hazard evaluation of renewable hydrogen/ammonia/air fuels. Energy 2018;159:252–63.
[42] CHEMKIN-Pro 19.2, Reaction Design, San Diego, California, 2017.
[43] Bradley D, Lawes M, Mansour MS. Explosion bomb measurements of ethanol–air laminar gaseous flame characteristics at pressures up to 1.4 MPa. Combust Flame 2009;156:1462–70.
[44] Bradley D, Sheppard CGW, Suardjaja IM, Woolley R. Fundamentals of high-energy spark ignition with lasers. Combust Flame 2004;138:55–77.

[45] Burke MP, Chen Z, Ju Y, Dryer FL. Effect of cylindrical confinement on the determination of laminar flame speeds using outwardly propagating flames. Combust Flame 2009;156:771–9.
[46] Vagelopoulos CM, Egolfopoulos FN. Direct experimental determination of laminar flame speeds. Proc Combust Inst 1998;27:513–9.
[47] Egolfopoulos FN, Zhu DL, Law CK. Experimental and numerical determination of laminar flame speeds: Mixtures of C2-hydrocarbons with oxygen and nitrogen. Proc Combust Inst 1991;23:471–8.
[48] Dayma G, Halter F, Dagaut P. New insights into the peculiar behavior of laminar burning velocities of hydrogen–air flames according to pressure and equivalence ratio. Combust Flame 2014;161:2235–41.
[49] Metghalchi M, Keck JC. Burning velocities of mixtures of air with methanol, isooctane, and indolene at high pressure and temperature. Combust Flame 1982; 48:191–210.
[50] Van Lipzig JP, Nilsson EJ, De Goey LP, Konnov AA. Laminar burning velocities of n-heptane, iso-octane, ethanol and their binary and tertiary mixtures. Fuel 2011; 90:2773–81.
[51] Chen Z, Tang C, Fu J, Jiang X, Li Q, Wei L, et al. Experimental and numerical investigation on diluted DME flames: Thermal and chemical kinetic effects on laminar flame speeds. Fuel 2012;102:567–73.
[52] Bechtold JK, Matalon M. The dependence of the Markstein length on stoichiometry. Combust Flame 2001;127:1906–13.
[53] Kim W, Sato Y, Johzaki T, Endo T, Shimokuri D, Miyoshi A. Experimental study on self-acceleration in expanding spherical hydrogen-air flames. Int J Hydrogen Energy 2018;43:12556–64.
[54] Oppong F, Zhongyang L, Li X, Xu C. Inherent instabilities in ethyl acetate premixed flames. Fuel 2021;290:120000.
[55] Mannaa O, Mansour MS, Roberts WL, Chung SH. Laminar burning velocities at elevated pressures for gasoline and gasoline surrogates associated with RON. Combust Flame 2015;162:2311–21.